

# Multimodel analysis on the response of the AMOC under an increase of radiative forcing and its symmetrical reversal

Giovanni Sgubin · Didier Swingedouw ·  
Sybren Drijfhout · Stefan Hagemann · Eddy Robertson

Received: 1 July 2014 / Accepted: 20 October 2014 / Published online: 5 November 2014  
© Springer-Verlag Berlin Heidelberg 2014

**Abstract** The response of the Atlantic meridional overturning circulation (AMOC) to an increase of radiative forcing (ramp-up) and a subsequent reversal of radiative forcing (ramp-down) is analyzed for four different global climate models. Due to changes in ocean temperature and hydrological cycle, all models show a weakening of the AMOC during the ramp-up phase. Once the external forcing is reversed, the results become model dependent. For IPSL-CM5A-LR, the AMOC continues its weakening trend for most of the ramp-down experiment. For HadGEM2-ES, the AMOC trend reverses once the external forcing also reverses, without recovering its initial value. For EC-EARTH and MPI-ESM-LR the recovery is anomalously strong yielding an AMOC overshoot. A robust linear dependency can be established between AMOC and density difference between North Atlantic (NA) deep water formation region and South Atlantic (SA). In particular, AMOC evolution is primarily controlled by a meridional salinity contrast between these regions. During the warming

scenario, the subtropical Atlantic becomes saltier while the NA experiences a net freshening which favours an AMOC weakening. The different behaviour in the models during the ramp-down is dependent on the response of the ocean at the boundaries of NA and SA. The way in which the positive salinity anomaly stored in the subtropical Atlantic during the ramp-up is subsequently released elsewhere, characterizes the recovery. An out-of-phase response of the salinity transport at 48°N and 34°S boundaries is able to control the meridional density contrast between NA and SA during the transient experiments. Such a non-synchronized response is mainly controlled by changes in gyre salinity transport rather than by changes in overturning transport, thus suggesting a small role of the salt advection feedback in the evolution of the AMOC.

**Keywords** Climate modelling · Global warming · Atlantic meridional overturning circulation · AMOC stability · Salt advection feedback · Reversibility

---

G. Sgubin · D. Swingedouw  
Environnements et Paléoenvironnements Océaniques et  
Continentalux (EPOC), Bordeaux, France

G. Sgubin (✉) · D. Swingedouw  
Institut Pierre Simon Laplace (IPSL), Paris, France  
e-mail: giovanni.sgubin@lsce.ipsl.fr

S. Drijfhout  
Royal Netherlands Meteorological Institute (KNMI),  
De Bilt, The Netherlands

S. Hagemann  
Max Planck Institute for Meteorology (MPI-M),  
Hamburg, Germany

E. Robertson  
Met Office Hadley Centre, Exeter, UK

## 1 Introduction

Given the massive amount of greenhouse gases released by human activities, which is probably doomed to further increase in the coming decades, the chances for the oceanic circulation systems such as the Atlantic meridional circulation overturning (AMOC) to experience future abrupt and irreversible change, as part or cause of general climate changes, is being increasingly discussed (Manabe and Stouffer 1993, 1995; Broecker 1997; Stocker and Schmittner 1997; Clark et al. 2002). The AMOC is essentially a meridional overturning cell which covers the entire Atlantic and crosses both hemispheres. More specifically it consists in (i) a sinking branch of dense water in North

Atlantic Deep Water (NADW) formation region, (ii) a deep southward water current, (iii) an upwelling in the southern Atlantic and (iv) a return branch in the upper ocean. By transporting heat northward all over the Atlantic basin (Trenberth and Caron 2001), the AMOC is a fundamental component of the global circulation system, which substantially regulates the interhemispheric heat exchanges (Ganachaud and Wunsch 2003; Johns et al. 2011). Any change in its structure would therefore have profound implications for climate not only in the Atlantic but at the global scale (Vellinga and Wood 2002; Zhang and Delworth 2005; Swingedouw et al. 2009). Alterations of global temperatures and hydrological cycle occurring in response to increasing greenhouse gases are currently modifying AMOC and its strength will likely undergo a decrease over the course of the 21st century (Schmittner et al. 2005). By analysing measurements at 25°N, Bryden et al. (2005) reported an AMOC decrease of about 35 % between 1957 and 2004. However, since the AMOC is affected by a seasonal variability, this value is likely to have been overvalued due to aliasing error in sampling measurements as shown by Kanzow et al. (2010). State-of-the-art atmosphere-ocean general circulation models (AOGCMs) also show a general weakening of the AMOC strength under increased greenhouse gases input for historical and future projections (Weaver et al. 2012). However, up to now, there is no indication of a total AMOC collapse within the end of the century, even if the meltwater from Greenland, not considered in AOGCMs, may play an important role (Swingedouw et al. 2006, 2007; Hu et al. 2011).

The question of whether the decrease of AMOC under anthropogenic emissions can eventually collapse, thus triggering abrupt climatic change, remains highly debated (Alley et al. 2003; Lenton 2011). The theory behind this discussion is based on the representation of the Earth's climate in terms of a deterministic dynamical system in which a bifurcation point (also named “tipping point”) can be crossed when a certain control parameter is changed. Lenton (2011) identified a series of critical climate subsystems (or “tipping elements”) in potential proximity of their threshold, beyond which they would abruptly shift to a qualitatively different state. Among them, the AMOC is one of the major candidates and an increase of freshwater flux (its classical control parameter) into the deep water formation region may potentially lead the AMOC towards a critical tipping point.

The risk of abrupt changes in AMOC strength is linked with its stability. Stommel (1961) suggested that the overturning circulation may operate in two “on” and “off” equilibrium modes under the same boundary conditions. By using a single hemisphere 2-box conceptual model for a density-induced overturning circulation, he analysed the equilibrium solutions of the NADW flow, finding a

typical hysteresis loop in the bifurcation diagram. In other words, under the same external freshwater forcing into the boxes, i.e. high-latitudes box and low-latitudes box, two stable states of NADW production (and its overturning circulation) were possible. In the bifurcation diagram, the stable “on” state solution is delimited by the position of the saddle-node bifurcation, the critical point beyond which it would abruptly turn into an “off” state. This non-linear behaviour is a direct consequence of a positive salt advection feedback for which any weakening of the overturning circulation would decrease the import of salinity in the high-latitudes region further decreasing the density difference between the boxes. Stommel's pioneering work set the basis for further similar investigations applied to more complex conceptual models, three-dimensional oceanic models and coupled ocean-atmosphere models (Rooth 1982; Bryan 1986; Manabe and Stouffer 1988; Rahmstorf 1996). In particular, by means of an interhemispheric Stommel-like model, Rahmstorf (1996) showed that the bistability of the AMOC depends on the net amount of freshwater flux due to the overturning cell entering the Atlantic at 34°S. This term, usually referred to as  $M_{OV}$ , is classically calculated as the baroclinic component of the zonally averaged freshwater flux at 34°S. Other analyses (de Vries and Weber 2005; Dijkstra 2007; Huisman et al. 2010; Hawkins et al. 2011), have shown that its sign is a good indicator for the potential existence of multiple AMOC equilibria in general circulation models. Dijkstra (2007) and Liu and Liu (2013) proposed the convergence of the freshwater transport accomplished by the AMOC, i.e.  $\Sigma = M_{OV}^{34^{\circ}S} - M_{OV}^{60^{\circ}N}$ , to be a more correct indicator. That is, if  $M_{OV}$  (or  $\Sigma$ ) is negative, i.e. positive salt advection feedback, any slowing of the AMOC would carry less salt within the deep convection region, thus reducing the formation of NADW and further braking the AMOC. Inverse model (Weijer et al. 1999) and direct observations (Huisman et al. 2010; Garzoli et al. 2013) showed a negative  $M_{OV}$ , thus supporting the hypothesis of a bistable regime for the present-day AMOC. However, Sijp et al. (2012) showed that this indicator could not be robust if the effects of the Antarctic Intermediate Water (AAIW) reverse cell on the Atlantic salt budget are significant. Intercomparisons between models of intermediate complexity (Rahmstorf et al. 2005; Hofmann and Rahmstorf 2009) confirmed the robustness of the hysteresis behaviour of the AMOC with respect to freshwater perturbations. However, up to now, except for some isolated cases (Hawkins et al. 2011), there is no wide-spread evidence for such a behaviour in more sophisticated state-of-the-art AOGCMs indicating that the AMOC is likely to be more stable than what simpler models exhibited. This can be explained by the fact that most of the AOGCMs show a positive sign of  $M_{OV}$  in

their pre-industrial conditions (Drijfhout et al. 2010) thus excluding the possibility of an “off” state AMOC. Furthermore, for those models exhibiting a negative  $M_{OV}$ , i.e. 40 % of the models considered by Weaver et al. (2012) under RCPs scenarios, one may infer that the salinity freshwater feedback is not the dominant process in establishing the AMOC evolution.

The possibility of a rapid change to the climate system raises the question as to whether that change is reversible. In a model study, Boucher et al. (2012) examined the reversibility of a wide range of climatic parameters under a symmetrical reversal of increased  $\text{CO}_2$  emissions. They showed unexpected hysteresis behaviours associated with cloud-coverage and stratification in the Southern Ocean. With a similar experimental design, Armour et al. (2011) found a fully reversible sea-ice cover, thus conjecturing about the nonexistence of a critical threshold for the sea-ice retreat. By linearly decreasing the  $\text{CO}_2$  concentration over 100 years from the stabilized level of the SRES A1B scenario (in which  $\text{CO}_2$  concentrations increased from a preindustrial value of 280–689 ppmv in 2100), Nakashiki et al. (2006) and Tsutsui et al. (2007) found a relatively fast response of surface conditions in the CCSM3 model, i.e. air temperature, precipitation and sea ice extent. On the other hand, the oceanic response, i.e. ocean mean temperature and steric sea-level rise, was significantly delayed. This was explained as an effect of the heat accumulated in the ocean interior during the period of increasing  $\text{CO}_2$ . Oceanic heat accumulation was also shown to be the cause of the hydrological hysteresis found by Wu et al. (2010) using the HadCM3 model in a ramp-up/ramp-down experiment. Bouttes et al. (2013) showed that global mean sea level rise due to an increase of  $\text{CO}_2$  emissions is, in principle, reversible. However, even if the thermal expansion anomaly were brought back to zero, the sea level would appear strongly altered in its spatial pattern. Wu et al. (2011) and Jackson et al. (2014) focused on the reversibility of the AMOC in different models and pointed out the possibility of an overturning circulation overshoot at the end of the forcing reversal. They explained this mechanism and its extent as connected to the build up of salinity in the subtropical Atlantic during the increasing  $\text{CO}_2$  phase.

The aim of the present paper is to further investigate the evolution of the AMOC under a global warming scenario and to study its reversibility under a symmetrical reversal of the external forcing. In order to gain insight on model dependency for this response, we use 4 different global models. The main issue handled concerns the identification of the exact mechanisms that drive the transient response of the AMOC. In particular we evaluate the impact of the stability state of the overturning circulation on its transient

behaviour, i.e. whether the salt advection feedback is a significant process in the transient experiments or whether other processes are of primary importance. The identification of the main model differences is also a matter of this paper.

Section 2 provides a description of the main features of the models as well as details of the experimental design adopted in this work. The general response of the AMOC is analyzed in Sect. 3. In Sect. 4 the mechanisms of AMOC recovery are examined in the different models by means of a salinity budget analysis within different sub-regions of the Atlantic basin. Finally, we propose a physical interpretation of the driving mechanisms leading to an AMOC overshoot. Section 5 outlines a summary of the most remarkable results carried out in this work.

## 2 Models and methods

### 2.1 Models

Outputs from four different models have been analysed, i.e. EC-EARTH, HadGEM2-ES, IPSL-CM5A-LR, MPI-ESM. The Table 1 summarizes their main features. All the models contribute to the fifth phase of the Coupled Model Intercomparison Project (CMIP5) (Taylor et al. 2012), the set of coordinated climate model experiments suggested for the fifth Assessment Report (AR5) of the Intergovernmental Panel on Climate Change (IPCC).

The European Community Earth system model (EC-EARTH) is a global climate system model developed by a consortium of 10 countries (Sterl et al. 2011). The current version, i.e. the 2.3 used for CMIP5 experiments, is based on the coupling of the Integrated Forecast System (IFS) of European Centre for Medium-Range Weather Forecasts (ECMWF), i.e. including atmospheric, chemistry, land and vegetation components, with the Nucleus for European Modelling of the Ocean (NEMO) for the ocean and sea-ice component. The atmospheric model IFS uses a T159 truncation which roughly corresponds to a horizontal resolution of 125 km, and 62 vertical levels. The oceanic model NEMO is a primitive equation model with a free surface. Discretization uses curvilinear Arakawa C-grid horizontally with a basic resolution of  $1^\circ$  and meridional refinements to the Equator up to  $1/3^\circ$ , while vertical axis consists in 40 z-levels.

The HadGEM2-ES has been designed at the Hadley Centre with the specific purpose of simulating long-term scale, i.e.  $O(10^2)$  years, climate evolution (Collins et al. 2011). It contains atmosphere, ocean, land, sea-ice as well as biogeochemical components. The atmospheric component (HadGAM2) has 38 z-levels extending to over 39 km in height, and a horizontal resolution of  $1.25^\circ \times 1.875^\circ$

**Table 1** Summary of the main features of the models used in our analysis

Model	Institute	Ocean	Atmosphere	References
EC-EARTH	Royal Netherlands Meteorological Institute	NEMO	IFS T159	Sterl et al. (2011)
	De Bilt, Netherlands	1°	1.25°	
		42 levels	62 levels	
HadGEM2-ES	Met Office	HadGOM2	HadGAM2	Collins et al. (2011)
	Hadley Centre	1°–1/3°	1.25° × 1.875°	
	Exeter, UK	40 levels	38 levels	
IPSL-CM5A-LR	Institute	NEMO	LMDZ5	Dufresne et al. (2013)
	Pierre Simon Laplace	2°	1.875° × 3.75°	
	Paris, France	31 levels	39 levels	
MPI-ESM-LR	Max Planck Institute	MPIOM	ECHAM6 T63	Giorgetta et al. (2013)
		1.5°	1.9°	
	Hamburg, Germany	40 levels	47 levels	

in latitude and longitude. The oceanic component (HadGOM2) uses a latitude-longitude  $360 \times 216$  grid with a zonal resolution of  $1^\circ$ , and a meridional resolution of  $1^\circ$  between the poles and the tropics and an increasing resolution up to  $1/3^\circ$  at the equator. The vertical grid consists of 40 unevenly spaced levels, which reduce to 10 m thickness near the surface.

The IPSL-CM5A-LR is a global general circulation model developed by the Institut Pierre Simon Laplace (Dufresne et al. 2013). The atmospheric component is based on the LMDZ5A model which, for the Low Resolution (LR) configuration, has  $96 \times 95$  grid points corresponding to a resolution of  $3.75^\circ \times 1.875^\circ$  and 39 vertical levels. The ocean and sea-ice component is based on the NEMOv3.2 model, with a horizontal resolution varying from  $0.5^\circ$  to  $2^\circ$  and 31 depth levels with thicknesses from 10 m near the surface to 500 at 5,000 m.

Developed at Max Planck Institute for Meteorology (MPI-M), the MPI-ESM-LR consists of the coupled general circulation models ECHAM6 for the atmosphere and MPIOM for the ocean, in combination with subsystem models for land, vegetation (JSBACH) and biogeochemistry (Giorgetta et al. 2013). The LR configuration uses a T63 horizontal resolution for the atmospheric component which are equivalent to  $1.9^\circ$ , and 47 hybrid  $\sigma$ -pressure levels. The MPIOM oceanic model consists in 40 z-levels over a bipolar grid with  $1.5^\circ$  resolution near the equator and higher resolution near the poles.

For all models, both Greenland and Antarctic ice sheet areas are fixed in time. Simple bucket parameterisations allow for closing the freshwater budget of the models by routing part of the snow accumulated over the ice sheet towards the ocean. Nevertheless, under a warming climate, when the ice sheet starts to lose mass and snow accumulation is lower than melting, no additional freshwater is released from the ice sheet in all the models, contrary to what was done in IPSL-CM4 in Swingedouw et al. (2006). Thus, the amount of

freshwater input associated with the ice sheet mass balance is only due to excess snow accumulation in the control run and does not account for additional freshwater release due to ice melt in a warming scenario. This freshwater input is therefore very modest in all the models considered here.

## 2.2 Experimental design

For the AR5, the IPCC proposed four different scenarios representing possible evolutions of the future greenhouse gas concentrations. These trajectories, following the CMIP5 protocol for the historical integration, i.e. 1850–2006, are named Representative Concentration Pathways (RCPs). They are referred to as RCP2.6, RCP4.5, RCP6 and RCP8.5 (Meinshausen et al. 2011) depending on their radiative forcing value in 2,100.

In the experiments here presented, the initial conditions are those produced by the historical simulations in the different models in 2006. The external radiative forcing consists of a ramp-up phase between 2006 and 2100 based on the RCP8.5 scenario. It is followed by a reversed phase, herein named ramp-down phase, in which the radiative forcing is decreased until 2195, when it recovers its initial value recorded in 2006 (Fig. 1). The changes in forcing concern greenhouse gases as well as ozone, aerosols and land-use changes. Those are all symmetrically reversed in the ramp-down phase. This experimental design is not intended to be a realistic projection of the future radiative forcing as a symmetrical reversal of radiative forcing is rather unlikely to occur; however, it allows for an investigation of the reversibility and inertia of the climatic system.

## 3 Results of the experiments

When comparing the 10-year averaged sea surface temperature (SST) field corresponding to the peak of external



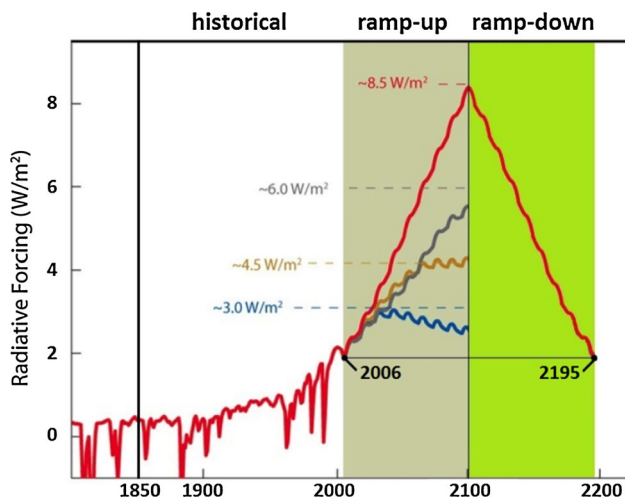


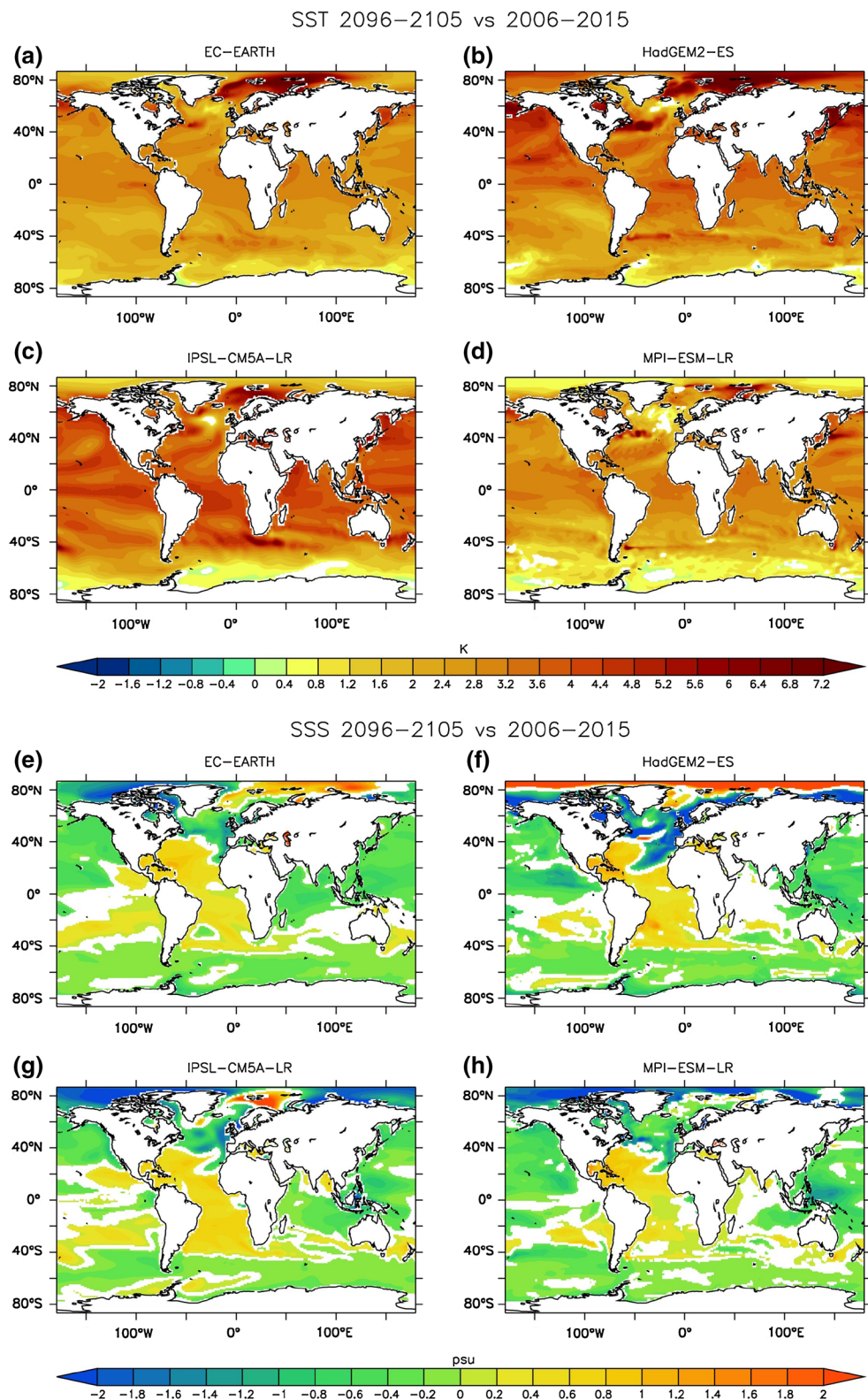
**Fig. 1** Radiative forcing (in  $\text{W/m}^2$ ) for the CMIP5 historical scenario (from 1850 to 2006), the CMIP5 RCPs scenarios (2006–2100), and the reversed RCP8.5 scenario (2100–2195). The red line indicates the radiative forcing used in the experiments presented here. For the ramp-up (grey-shaded) phase, i.e. 2100–2195, radiative forcing follows the RCP8.5 scenario, which is symmetrical reversed for the ramp-down (green-shaded) phase, i.e. 2100–2195. The initial conditions used for the different models coincide with the final outputs of the respective historical simulations

radiative forcing (2096–2105) with the 10-year averaged field at the beginning of the experiments (2006–2015), a general increase of SST is evidenced (Fig. 2a–d). The rise of radiative forcing leads, for all the models, to a positive SST anomaly which generally spreads all over the globe with maximum increase localized in the polar regions of the Northern Hemisphere. The averaged amount of global SST anomaly among the models at the end of the ramp-up experiments is  $2.87 \pm 0.39$  K. Changes in Sea Surface Salinity (SSS) are also similar in all the models but more heterogeneous in their pattern (Fig. 2e–h). During the ramp-up, salinification of the ocean surface is mainly concentrated in the tropical and subtropical Atlantic, roughly between  $40^\circ\text{N}$  and  $40^\circ\text{S}$ , while the rest of the globe experiences a general freshening. The general accumulation of salt in the tropical region of the Atlantic enhances its salinity contrast with other regions, notably with the subpolar North Atlantic. At the end of ramp-up phase, the sea surface in the Atlantic region north of  $40^\circ\text{N}$  experiences an averaged freshening of  $0.71 \pm 0.13$  psu while the subtropical surface becomes  $0.29 \pm 0.04$  psu saltier. We suggest that the change in the hydrological cycle under the warming scenario is responsible for this pattern. An increase of net evaporation in the tropical Atlantic (which will be documented in the next section) generates a considerable salinification in this region. By contrast, more precipitation freshen the subpolar region in the North Atlantic (NA), as well as in the Pacific Ocean and in the

Indian Ocean, while Southern Ocean is less affected by SSS changes. Both the warming and the freshening concentrated in the subpolar NA produce a decrease of surface density in this region.

The spatial pattern of the reversibility of SST and SSS can be detected by plotting their anomalies at the end of the ramp-down (averaged field between 2186–2195) with respect to the 10-year averaged initial fields (Fig. 3). The reversal of radiative forcing causes a general decrease of SST, which can be seen in each model by comparing Figs. 2a–d and 3a–d. However, apart from some limited regions, the SST does not recover its initial values, the final SST being generally higher than the initial conditions. The amount of the residual global SST positive anomaly in 2195 is  $0.97 \pm 0.22$  K. In agreement with Nakashiki et al. (2006), Tsutsui et al. (2007) and Wu et al. (2010), this is due to the higher inertia of the oceanic system whose response is delayed with respect to the external forcing. Moreover, Fig. 3b, c show a partial cooling south-east of Greenland for HadGEM2-ES and IPSL-CM5-LR. This may be associated to the so-called North Atlantic warming hole, a behaviour already evidenced in measurements (IPCC 2013) and model results (Drijfhout et al. 2012). On the other hand, SSS behaves in different ways depending on the model. In EC-EARTH and MPI-ESM-LR (Fig. 3e, h), the freshening experienced by the subpolar NA during the ramp-up phase is completely cancelled and the deep water formation region becomes increasingly saltier at the surface exceeding its initial values. The tropical Atlantic generally remains saltier when compared with the initial pattern while the Indian and the Pacific sectors remain fresher. However, a comparison between Figs. 2e, h and 3e, h clearly shows an inversion of the SSS trend for these regions, without completely recovering the initial conditions. In other words, while the subpolar NA experiences a fast re-establishment of the initial conditions, the response of the rest of the ocean to the reversal of external forcing is slower. In HadGEM2-ES there is just a partial and weak recovery of the initial SSS. The most evident difference with the former two models is that the deep water formation region remains generally less salty when compared with the initial pattern. In contrast with all the others model results, during the ramp-down the SSS in IPSL-CM5A-LR seems qualitatively to persist in the configuration found for the peak of ramp-up phase, with a saltier mid-Atlantic and a fresher subpolar NA. This can be inspected by comparing the SSS pattern in Fig. 2g, where no large difference can be found in the general structure of the Atlantic SSS anomalies. To summarize, we assess that all the models respond qualitatively in a similar way to an increase of radiative forcing. On the contrary, model differences arise once the external forcing is reversed. These differences notably concern the response of SSS in the NA deep water formation

**Fig. 2** Difference between 10-year averaged sea surface temperature (SST) at the end of the ramp-up phase (2095–2104) and initial 10-year averaged fields (2006–2015) for **a** EC-EARTH; **b** HadGEM2-ES; **c** IPSL-CM5A-LR; **d** MPI-ESM-LR, and for sea surface salinity (SSS) in **e** EC-EARTH; **f** HadGEM2-ES; **g** IPSL-CM5A-LR; **h** MPI-ESM-LR. Only differences which are statistically significant at the 95 % confidence level are shown



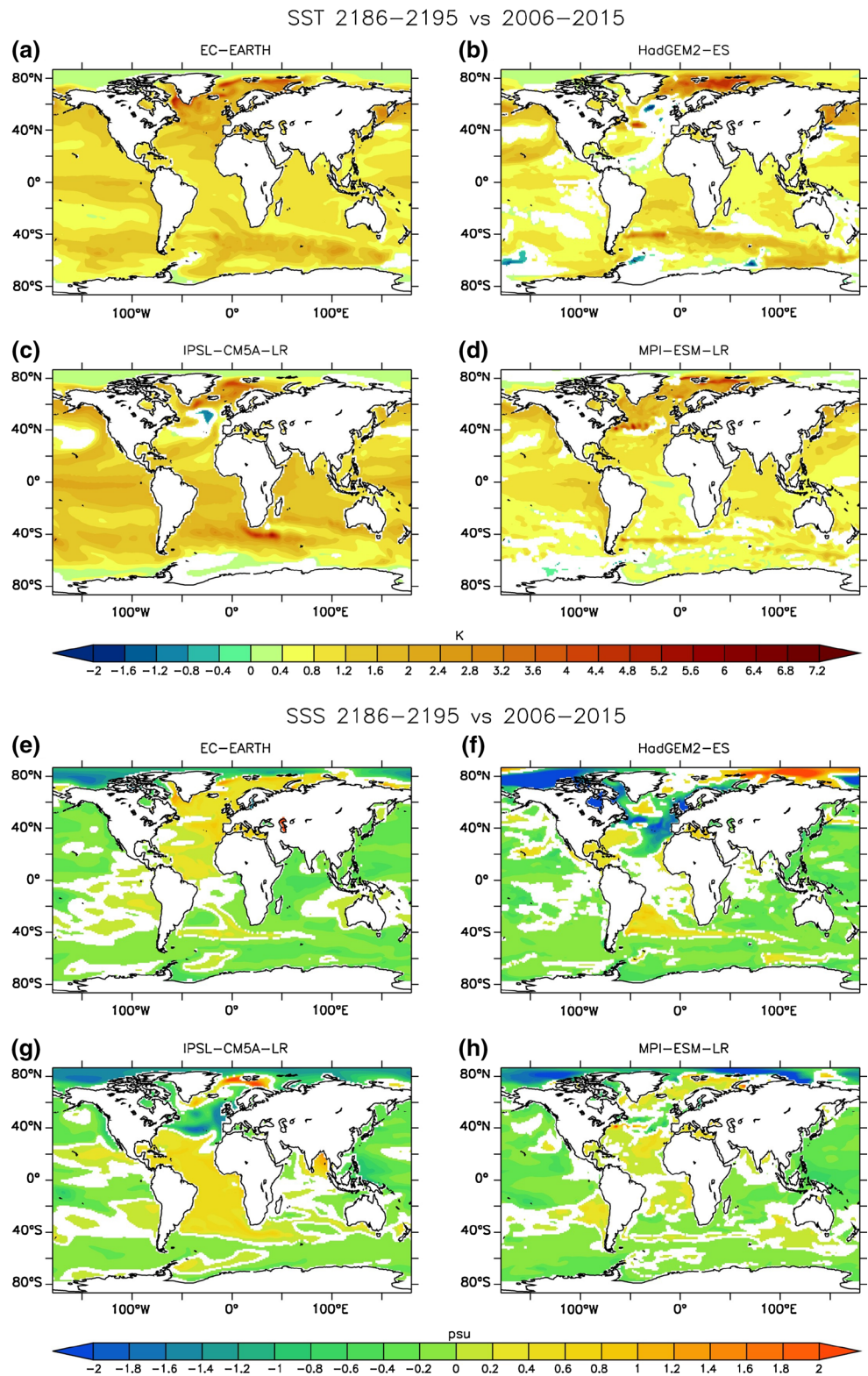
region, in which two models show a positive anomaly at the end of the simulation, while the other two can not rebalance the loss of salinity in the region which occurred during the ramp-up phase.

### 3.1 Response of the AMOC

We define AMOC-indices by the annual mean maximum of the Atlantic meridional overturning streamfunction.



**Fig. 3** Difference between 10-year averaged SST at the end of the ramp-down phase (2186–2195) and initial 10-year averaged fields (2006–2015) for **a** EC-EARTH; **b** HadGEM2-ES; **c** IPSL-CM5A-LR; **d** MPI-ESM-LR, and for SSS in **e** EC-EARTH; **f** HadGEM2-ES; **g** IPSL-CM5A-LR; **h** MPI-ESM-LR. Only differences which are statistically significant at the 95 % confidence level are shown



Different indexes, i.e. at 48°N, at 26°N and maximum between 60°N and 30°S, have been plotted in Fig. 4. As one may expect, when the radiative forcing increases, the AMOC decreases in all experiments due to weaker deep

convection caused by a less dense subpolar NA surface water (Swingedouw et al. 2007). At the end of the ramp-up phase, the amount of the AMOC reduction is roughly about 25 % of its initial value for EC-EARTH and MPI-ESM-LR

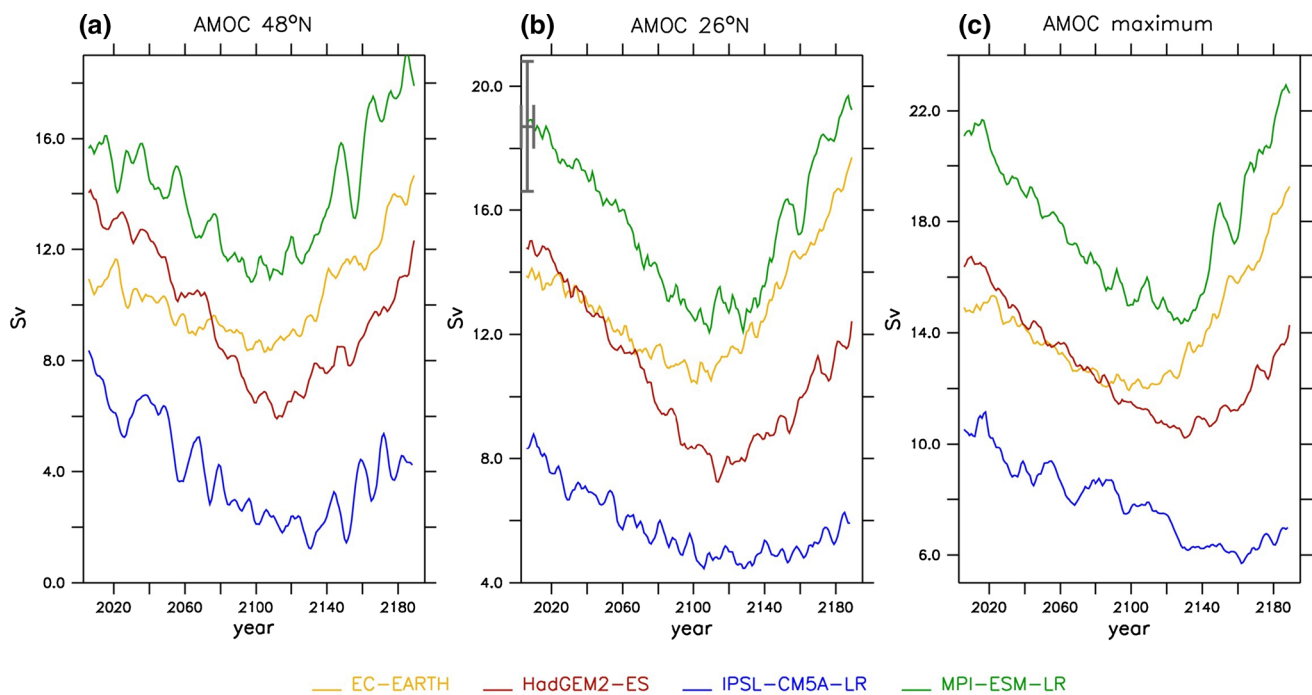


**Fig. 4** Different AMOC indices: **a** at 48°N, **b** at 26°N, **c** maximum index, for EC-EARTH (orange line), HadGEM2-ES (red line), IPSL-CM5A-LR (blue line) and MPI-ESM-LR (green line). The gray bar

at the beginning of **b** indicates the observed value of AMOC at 26°N by Kanzow et al. (2010)

and about 35 % for the HadGEM2-ES and IPSL-CM5A-LR. It is also worth pointing out that only MPI-ESM-LR has an initial value of AMOC that matches the range of observed data at 26°N (Kanzow et al. 2010). The ramp-down forcing restores the AMOC in EC-EARTH and MPI-ESM-LR to the point of even exceeding the value in 2006. The maximum amount of this overshoot can be roughly quantified as 10 % for MPI-ESM-LR and 30 % for EC-EARTH with respect to their initial values. In contrast, AMOC strength does not totally recover in HadGEM2-ES which however shows an inversion in the trend once the external forcing is reversed. The most striking result is the one concerning IPSL-CM5A-LR for which the AMOC seems to further decrease even during the ramp-down phase. However, starting from 2140, hints of a reversing trend are visible for the AMOC.

During the ramp-up, the decline of the AMOC theoretically leads to a reduction of northward ocean heat transport (Bryden et al. 2014). However, until 2100, none of the models show a cooling in the North Atlantic. This is likely due to the dominant role of the global warming caused by the external radiative forcing. Nevertheless, during the ramp-down, a slight cooling arises south-east of Greenland for HadGEM2-ES and IPSL-CM5A-LR, thus indicating a lagged-response between temperature anomalies directly induced by radiative forcing and oceanic re-adjustments. Furthermore, the absence of a cooling in the NA for

EC-EARTH and MPI-ESM-LR is likely to be attributed to the overshoot of the AMOC, which transports northward an exceeding quantity of heat during the ramp-down, if compared to the initial state. This is in agreement with Wu et al. (2011), who showed an AMOC overshoot producing a 3.5 K warming in the subpolar NA.

The formation of NADW is a key element of the meridional overturning cell (Swingedouw et al. 2007). It depends on the density budget in the northern North Atlantic, insofar as a decline of the surface density in this region would weaken the amount of sinking. Such a decline can be induced both by a warming and/or by a freshening of the surface waters. In relation to Fig. 2, both a warming and a freshening of the subpolar North Atlantic during the ramp-up likely drive an AMOC weakening (Gregory et al. 2005). The partial restoring of the SST during the ramp-down phase (Fig. 3a–d) may drive a partial recovery of the surface density in the deep water formation region. On the other hand, the different responses found for the SSS (Fig. 3e–h) can ultimately determine the total surface density budget in the convection region, yielding different responses for the AMOC. As it will be demonstrated in Sect. 4, the salinity budget in the North Atlantic is the effective component in supporting a stronger or weaker recovery of the AMOC, with overshoot that can take place despite the temperature remaining warmer with respect to its initial value.

### 3.2 Analysis of the stability of the AMOC

In our 190-year experiments, even though the overturning circulation constantly weakens under the warming scenario, none of the models show any AMOC abrupt collapse. Moreover, all the models but one, i.e. IPSL-CM5A-LR, clearly exhibit a qualitative recovery of the AMOC once the radiative forcing is reversed. For IPSL-CM5A-LR this issue is more delicate: Fig. 4 shows that, on the whole, the AMOC decreases even during part of the ramp-down phase. However, the limited integration time does not allow to assess whether the AMOC goes towards a new equilibrium configuration (which can also be an “off” state) or if this model is simply more inertial, meaning that a longer period is needed for the AMOC to recover. In this context, the analysis of the stability of the AMOC can shed light on the mechanisms underlying the different behaviours found in the model outputs.

The potential bistability of the AMOC in a conceptual Stommel-like models essentially arises because mixed boundary conditions make the governing equations of the overturning flow a nonlinear system, with multiple equilibria solutions (Stommel 1961; Rahmstorf 1996). The validity of the bifurcation diagram is based on the assumption that the overturning flow is proportional to a density difference between northern and southern boxes.

In order to draw an analogy between a Stommel-like conceptual model, with reference to the interhemispheric box model described by Rahmstorf (1996), the full-depth Atlantic is divided into three boxes: a North Atlantic (NA) roughly between 48°N and 75°N, a South Atlantic (SA) box between 55°S and 34°N, and a Mid-Atlantic (MA) box in between them as illustrated in Fig. 5. We indicate the NA and MA as forming the *Atlantic catchment*, i.e. the part of the Atlantic embedded by continents. The NA limits are chosen such that the NADW formation region is approximately covered, whereas the choice of the SA can theoretically have different dimensions. Here its northern border coincides with the southern limit of the Atlantic catchment, while the southern border coincides with the latitude of Cape Horn.

By examining the evolution of the density contrast between NA and SA  $\Delta\rho_{NA-SA}$  and comparing it with the AMOC indexes  $\psi_{AMOC}$  over the 190 years of our experiments, a significant correspondence (correlation of more than 0.78) in all models has been found (Table 2). Therefore, it can be asserted that

$$\psi_{AMOC} \propto \Delta\rho_{NA-SA} = \rho_{NA} - \rho_{SA}. \tag{1}$$

This legitimates the conceptual validity of the stability analysis in terms of a salt advection feedback. That is, in an interhemispheric Stommel-like box model, the bistability of the AMOC depends on the freshwater flux due to the overturning cell at the southern border of the Atlantic

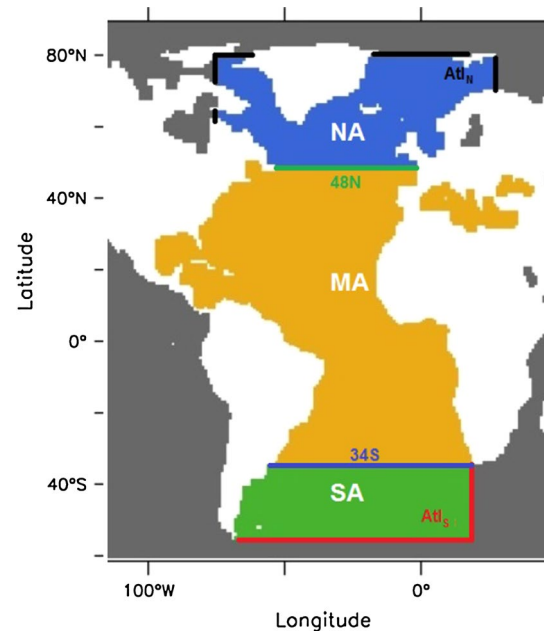


**Fig. 5** Division of the Atlantic Ocean into three boxes: (blue box) North Atlantic (NA), (orange box) Mid-Atlantic (MA) and (green box) South Atlantic (SA). The boundaries of each boxes are named in the following way: (black contour) Northern limit of the Atlantic (Atl<sub>N</sub>), (green contour) boundary at 48°N (48N), (blue contour) boundary at 34°S (34S) and (red contour) Southern limit of the Atlantic (Atl<sub>S</sub>)

catchment (Rahmstorf 1996). If at 34°S the overturning circulation exports freshwater out of the basin, i.e.  $M_{OV} < 0$ , any slowing would decrease the salinity in the basin. In this way the deep convection region would also be affected by a reduction of NADW formation and a consequent further slowing down of the AMOC.

Here, the evolution of  $M_{OV}$ , has been calculated for all models. It is defined as the baroclinic component of the zonally averaged meridional freshwater transport across the vertical section at 34°S. If we consider a generic surface  $\partial\Omega$ , we can define the volume transport across  $\partial\Omega$  as

$$T_{\partial\Omega} = \iint_{\partial\Omega} \mathbf{u}_N \cdot \hat{n} \, ds \tag{2}$$

and the net equivalent freshwater transport across  $\partial\Omega$  as

$$M_{\partial\Omega} = -\frac{1}{S_0} \iint_{\partial\Omega} S \mathbf{u}_N \cdot \hat{n} \, ds \tag{3}$$

where  $ds$  is the infinitesimal surface,  $S$  is the salinity,  $\mathbf{u}_N$  is the normal outflow velocity,  $S_0 = \iint_{\partial\Omega} S \, ds / \iint_{\Omega} ds$  and  $\hat{n}$  is the oriented outward pointing unit normal field of the surface whose positive standard directions  $\hat{x}, \hat{y}, \hat{z}$  in the models grids are respectively E, N and zenith directions. As detailed in Drijfhout et al. (2010),  $M_{OV}$  can be derived by expressing  $M$  calculated at the vertical section of 34°S as:



**Table 2** Correlation between AMOC strength and meridional density gradient between NA and SA boxes as defined in Fig. 5 computed over the 190 years of simulation

Model	AMOC	
	Maximum	48°N
EC-EARTH	0.96	0.91
HadGEM2-ES	0.91	0.89
IPSL-CM5A-LR	0.78	0.87
MPI-ESM-LR	0.83	0.87

$$\begin{aligned}
 M_{34} &= -\frac{1}{S_0} \iint_{34S} vS \, dx \, dz \\
 &= -\underbrace{\frac{1}{S_0} \iint_{34S} \bar{v}\bar{S} \, dx \, dz}_{T_{34}} - \underbrace{\frac{1}{S_0} \iint_{34S} v^*\bar{S} \, dx \, dz}_{M_{OV}} \\
 &\quad - \underbrace{\frac{1}{S_0} \iint_{34S} v'S' \, dx \, dz}_{M_{AZ}}
 \end{aligned}
 \tag{4}$$

after the decomposition of the generic variable  $f$ , i.e.  $v$  and  $S$ , into

$$f = \bar{f} + f' = \tilde{f} + f^* + f' \tag{5}$$

in which  $\bar{f} = \int f \, dx / \int dx$  is the zonal mean,  $f' = f - \bar{f}$  is the azonal component,  $\tilde{f} = \iint f \, dx \, dz / \iint dx \, dz$  is the barotropic part of the zonal mean and  $f^* = \bar{f} - \tilde{f}$  is the baroclinic part. The total freshwater transport across 34°S is therefore divided into the zonally averaged baroclinic component  $M_{OV}$  associated with the overturning circulation, and the wind-driven component, which depends on the volume transport  $T_{34}$ , and on the azonal term  $M_{AZ}$ . The latter, i.e. the third component of the right side of Eq. 5, is related

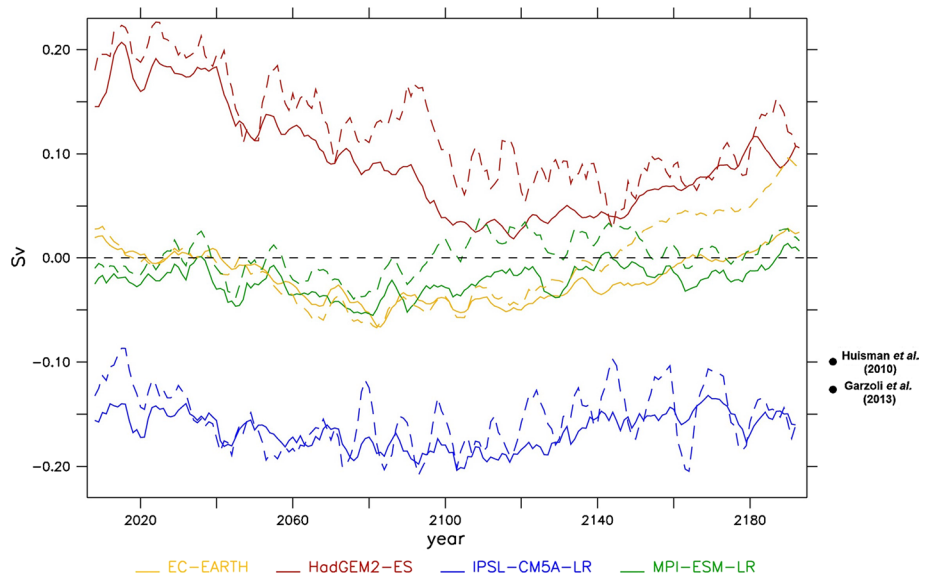
to zonal variations of velocity and salinity arising from the gyre circulation and eddies. Since the Atlantic is a net evaporative basin, a positive value of  $M_{34}$  is expected, i.e. a net freshwater influx within the Atlantic catchment. Nevertheless, in equilibrium conditions,  $M_{OV}$  can be negative if the azonal freshwater import at 34°S exceeds the freshwater loss due to evaporation in the basin.

The evolution of the bistability indicator  $M_{OV}$  for each of the models is shown in Fig. 6. In HadGEM2-ES,  $M_{OV}$  is positive throughout the length of the experiment, evidencing a negative salt advection feedback and a theoretical monostable regime. For EC-EARTH and MPI-ESM-LR,  $M_{OV}$  swings around (slightly) positive and negative values. Therefore, following the nomenclature adopted by Weaver et al. (2012), it can be said that they show multiple regime states (monostable and bistable). The IPSL-CM5A-LR model, by contrast, conceptually lies in a bistable regime as the indicator  $M_{OV}$  is always negative. This value is closest to observation-based estimates (Weijer et al. 1999; Huisman et al. 2010; Garzoli et al. 2013). The negative sign for the current  $M_{OV}$  can indicate proximity of the present climate state to a tipping point. It also seems to influence the transient AMOC response. Indeed, a positive salt advection feedback may inhibit its recovering process, which can either not take place or occur over a longer time scale. In order to measure the impact of the salt advection feedback in the different model responses, we quantify its influence in determining the AMOC evolution.

### 4 Mechanisms of AMOC recovery

Given the good correlation between AMOC and NA–SA meridional density gradient (Table 2), we calculate the

**Fig. 6** Evolution of  $M_{OV}$  in EC-EARTH (orange line), HadGEM2-ES (red line), IPSL-CM5A-LR (blue line) and MPI-ESM-LR (green line). The corresponding evolution of the  $\Sigma$  indicator proposed by Dijkstra (2007) and Liu and Liu (2013) is shown by the dashed line. The black points on the right indicate the climatological estimate from observed data from Huisman et al. (2010) (−0.1 Sv) and Garzoli et al. (2013) (−0.16 Sv)



density budget within the different boxes in order to understand how the AMOC recovers. We also compute the respective thermal and haline contributions under linear assumption, expressed as

$$\Delta\rho = \alpha\Delta T + \beta\Delta S, \tag{6}$$

where  $\alpha$  and  $\beta$  are respectively the thermal expansion and haline contraction coefficients. In all models, the NA generally freshens and warms during the ramp-up and, as a consequence, the density decreases (Fig. 7a). The partial recovery during the ramp-down is mainly due to an increase of salinity, while temperature still contributes in reducing density. In the MA, despite a general salinification during the ramp-up, the density decreases under the effect of an increasing temperature. Temperature is also the main component in determining the partial restoration of the initial density in the region during the ramp-down phase (Fig. 7b). In the SA, the haline contribution is of second order compared to the thermal one, which primarily determines the density evolution over the whole experiment (Fig. 7c). The resulting overall meridional density contrast (lower panels of Fig. 7) generally weakens during the ramp-up and reinforces during the ramp-down. In particular, for EC-EARTH and MPI-ESM-LR (first and fourth columns of Fig. 7), where an overshoot of the AMOC occurs, the  $\Delta\rho_{NA-SA}$  exceeds its initial value at the end of the simulation as a consequence of a markedly asymmetric haline response. This is mainly driven by an anomalously strong salinity increase within the NA. Such a strong input of salt does not take place in HadGEM2-ES and IPSL-CM5A-LR, where the NA remains fresher (and warmer) and the meridional density contrast weaker (second and third columns of Fig. 7).

Since the haline contribution is the main component in determining the  $\Delta\rho_{NA-SA}$  as well as the inter-model differences, we focus on salinity anomalies within NA, MA and SA. These are mainly controlled by changes in hydrological cycle and consequent advective adjustments. In Fig. 8, the net sea surface water flux (EPRI) anomalies in NA, MA and SA have been plotted. This term also includes mass exchange with sea ice at high latitudes. A preliminary sketch of inter-boxes mutual salinity exchange may be summarized as follows: during the ramp-up process, the increase of precipitation and river runoff in the NA (Fig. 8a) is such that this region experiences a net freshening (upper panels in Fig. 7). At the same time, the salinity in the MA grows as the consequence of a higher net evaporation in this region (Fig. 8b). On the other hand, the SA is slightly affected by changes in the hydrological cycle (Fig. 8c), thus the salinity remains nearly constant. The additional salinity in the MA represents a potential source that can be advected northward or southward during

the recovery process once the external forcing is reversed. The way in which MA redistributes the salinity anomaly in NA and SA is central in determining the AMOC response as it can eventually drive an anomalously strong rise of the NA–SA salinity contrast.

#### 4.1 Equivalent freshwater budget in the Atlantic

In order to interpret the differences between the models and to understand the physical mechanisms determining the AMOC overshoot, we diagnose the salinity budget in terms of equivalent freshwater fluxes in NA, MA and SA and we distinguish the contribution from the single components.

If one considers a volume of ocean  $\Omega$ , the equation of salt conservation reads

$$\underbrace{\iiint_{\Omega} \frac{\partial S}{\partial t} d\omega}_{\text{salt changes}} = - \underbrace{\iint_{\partial\Omega} S \mathbf{u}_N \cdot \hat{n} ds}_{\text{salt advection}} - S_{\Omega} \underbrace{\frac{\partial}{\partial t} \iiint_{\Omega} d\omega}_{\text{volume changes}} + \underbrace{\iint_{\partial\Omega} \nu \cdot \nabla S ds}_{\text{salt diffusion}} \tag{7}$$

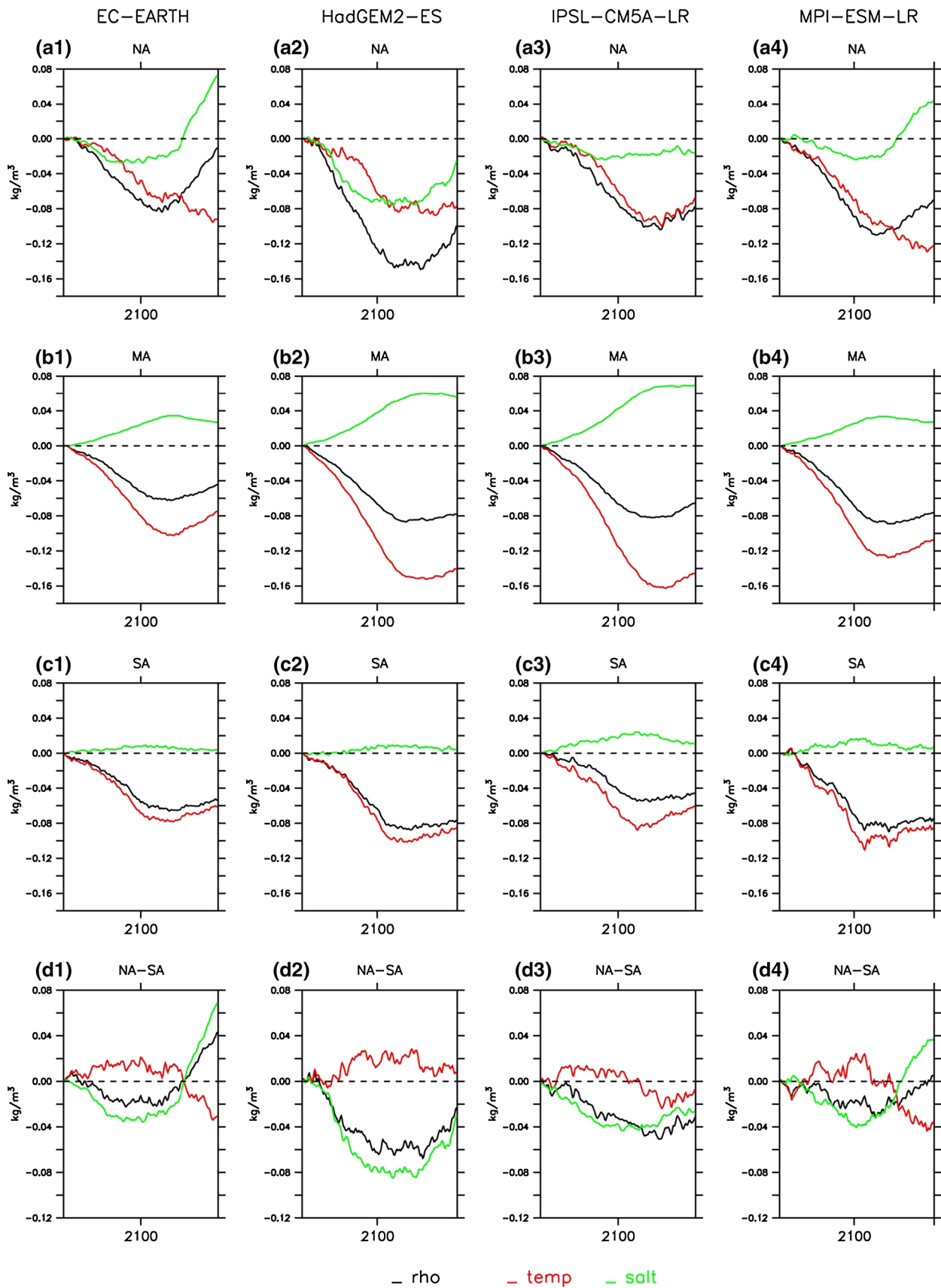
where  $\partial\Omega$  is the boundary of the ocean portion  $\Omega$ ,  $d\omega$  and  $ds$  are respectively the infinitesimal volume and the infinitesimal surface,  $S$  is the salinity,  $\mathbf{u}_N$  is the normal velocity,  $\hat{n}$  is the oriented unit vector,  $S_{\Omega} = \iiint_{\Omega} S d\omega / \iiint_{\Omega} d\omega$  and  $\nu$  is the diffusion tensor. In a full-depth portion of the ocean,  $\mathbf{u}_N$  is equal to the horizontal velocity  $\mathbf{u}_H$  and the second term on the right side of Eq. 7 becomes (under the Boussinesq approximation)

$$\begin{aligned} -S_{\Omega} \frac{\partial}{\partial t} \iiint_{\Omega} d\omega &= -S_{\Omega} \iint_{z=\eta} \frac{\partial \eta}{\partial t} ds \\ &= S_{\Omega} \left( \iint_{\partial\Omega} \mathbf{u}_H \cdot \hat{n} ds + \iint_{z=\eta} \text{EPRI} ds \right) \end{aligned} \tag{8}$$

where  $\eta$  is the free surface elevation and EPRI is the net outgoing volume flux of freshwater per unit time per unit area normal to ocean surface. If we divide the salt budget in Eq. 7 by  $-S_{\Omega}$  we obtain an equivalent freshwater budget, which, by taking into account Eqs. 8 and 3, becomes:

$$\begin{aligned} -\frac{1}{S_{\Omega}} \iiint_{\Omega} \frac{\partial S}{\partial t} d\omega &= \frac{1}{S_{\Omega}} \iint_{\partial\Omega} S \mathbf{u}_H \cdot \hat{n} ds - \iint_{\partial\Omega} \mathbf{u}_H \cdot \hat{n} ds \\ &\quad - \iint_{z=\eta} \text{EPRI} ds - \frac{1}{S_{\Omega}} \iint_{\partial\Omega} \nu \cdot \nabla S ds. \end{aligned} \tag{9}$$

With reference to the terminology introduced in Fig. 5, under the approximation  $S_{\Omega} = S_0$  and taking into account Eqs. 2, 3 and 9, the equivalent freshwater budget within the NA, MA and SA calculated on the model grids are respectively



◀ **Fig. 7** Time series of the density difference in kg/m<sup>3</sup> (black line) and its contribution from temperature (red line) and salinity (green line) for NA (a), MA (b), SA (c) and difference between NA and SA (d) for EC-EARTH (first column), HadGEM2-ES (second column), IPSL-CM5A-LR (third column) and MPI-ESM-LR (fourth column)

$$\begin{aligned}
 M_t^{NA} &= \Delta M_{48N} - \Delta M_{AtlN} - EPRI^{NA} + r^{NA} \\
 M_t^{MA} &= \Delta M_{34S} - \Delta M_{48N} - EPRI^{MA} + r^{MA} \\
 M_t^{SA} &= \Delta M_{AtlS} - \Delta M_{34S} - EPRI^{SA} + r^{SA}
 \end{aligned}
 \tag{10}$$

where  $M_t^\Omega$  indicates the freshening trend in the box  $\Omega$ ,  $\Delta M_{\partial\Omega} = M_{\partial\Omega} + T_{\partial\Omega}$  is the net freshwater influx accomplished by advection at the lateral surface  $\partial\Omega$ , and the terms  $r^\Omega$  are the residuals that take into account diffusion and interpolation errors that may arise since the budget is diagnosed in discretised models.

Figure 9 summarizes the average contribution by all terms in Eq. 10 during the ramp-up and the ramp-down simulations. In the NA, precipitation and freshwater advection from the north are mainly balanced by a salinity inflow at 48°N (boundary between NA and MA). During the warming scenario, the net decrease of upward EPRI (Fig. 8a) leads to a general freshening in the region as the oceanic adjustments are not able to counterbalance such an atmospheric change. During the ramp-down phase, NA experiences either a partial (in HadGEM2-ES and

IPSL-CM5A-LR) or an overshooting (in EC-EARTH and MPI-ESM-LR) salinity restoration. Since the total contribution from EPRI to the salinity budget is roughly equal over the ramp-up and the ramp-down, such a net salinification during the ramp-down is mainly driven by changes in advected freshwater at the NA boundaries. In the MA, the net evaporation competes with freshwater imports at 48°N and 34°S in determining the salinity budget. The increase of net evaporation in the region (Fig. 8b) during the ramp-up experiments is not balanced by a correspondent salt export at the boundaries and the MA becomes saltier. The reversed radiative forcing triggers a partial freshening in the MA for EC-EARTH and MPI-ESM-LR while for HadGEM2-ES and IPSL-CM5A-LR the salinity comprehensively continues to increase during the ramp-down phase. In the SA, an influx of freshwater caused by a net negative EPRI and by exchanges with the Southern Ocean balances an export of freshwater to the MA at 34°S. SA is just slightly affected by changes in the hydrological cycle (Fig. 8c) and no significant trend has been evidenced during the ramp-up/ramp-down experiments.

For our experimental design, the external forcing is purely symmetrical in time with respect to 2100. Figure 9 shows that the advective terms ( $\Delta M_{\delta\Omega}$ ) over the ramp-down experiments clearly differ from those over the ramp-up phase, evidencing an asymmetric response with respect to 2100. The degree of temporal asymmetry (hereinafter  $A_t$ )

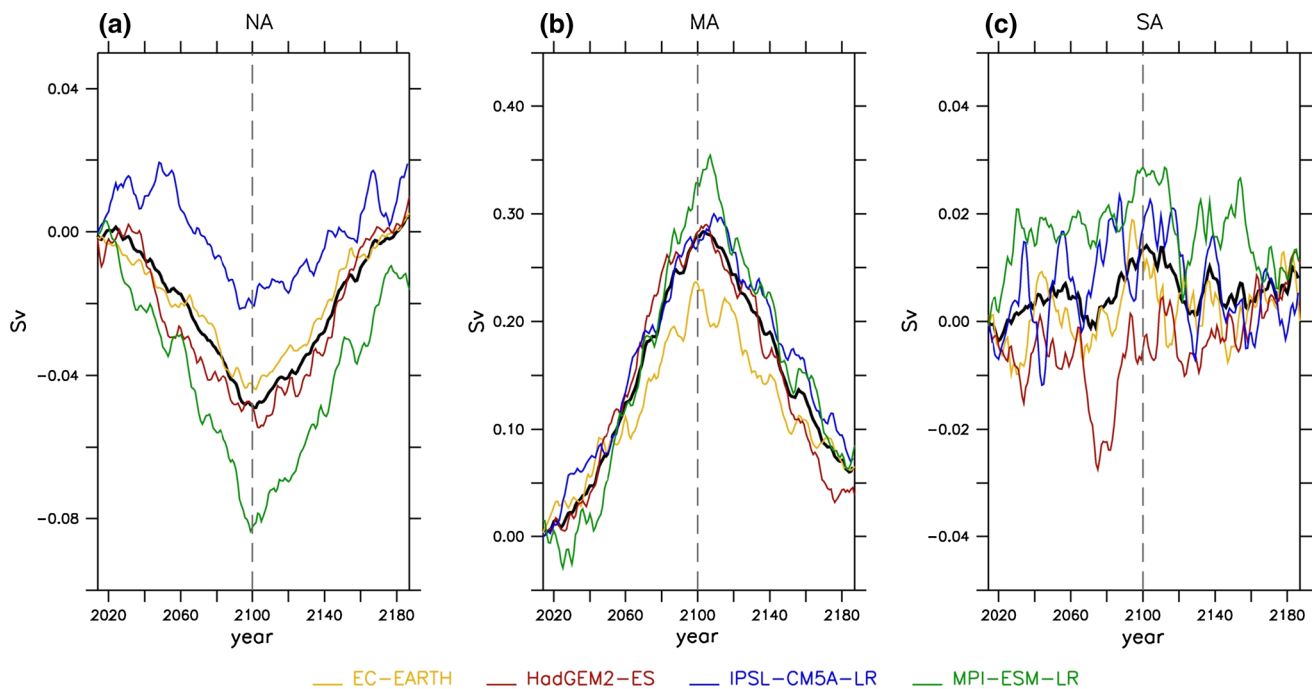
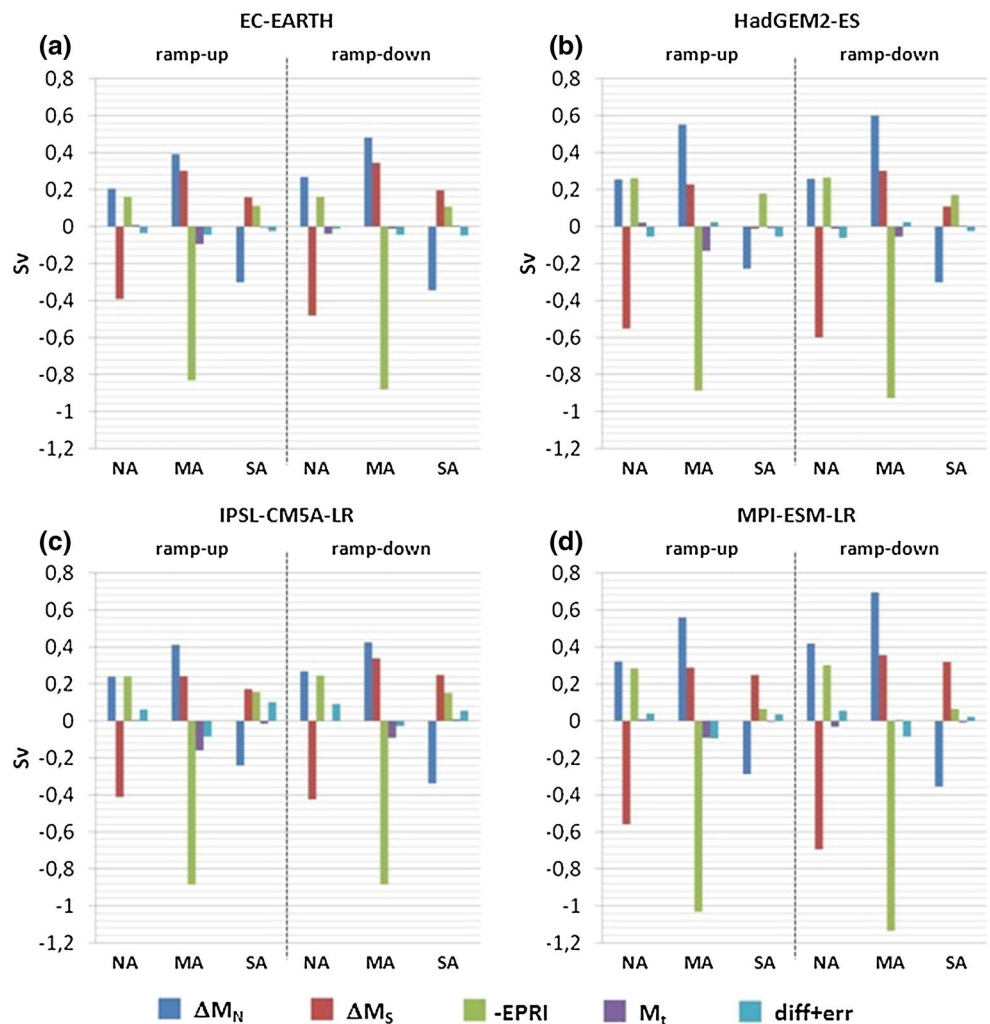


**Fig. 8** Net (upward) water flux at the sea surface (E-P-R-I) anomaly in Sv within a) the NA, b) the MA and c) the SA for EC-EARTH (orange lines), HadGEM2-ES (red lines), IPSL-CM5A-LR (blue

lines) and MPI-ESM-LR (green lines). The black line indicates the ensemble between the 4 models

**Fig. 9** Freshwater budget in the NA, MA and SA regions as detailed in Eq. 10 for **a** EC-EARTH; **b** HadGEM2-ES; **c** IPSL-CM5A-LR; **d** MPI-ESM-LR. All the components are expressed in Sv. The subscripts *N* and *S* represent respectively the northern and southern limits of each box over which the transports are calculated. By adopting the nomenclature of Fig. 5, *N* (*S*) stands for  $Atl_N$  (48°N) in NA, 48°N (34° S) in MA and 34°S ( $Atl_S$ ) in SA. They correspond to  $\Delta M_N$  (blue bar) and  $\Delta M_S$  (red bar). Along with EPRI (green bar) and diffusion plus error term (cyan bar), they characterize the freshening trend  $M_t$  (violet bar). The budget is calculated both for the ramp-up phase (left side of each panel) and for the ramp-down phase (right side of each panel) by using averaged data



with respect to 2100 of the generic component  $f$  on the right-hand side of Eq. 10 can be extracted by subtracting the total (or the averaged) amount of freshwater influx in Eq. 10 over the ramp-up period from the one over the ramp-down period

$$A_t(f) = \bar{f}^{DW} - \bar{f}^{UP} = \int_{t=2101}^{t=2195} f(t)dt - \int_{t=2006}^{t=2100} f(t)dt, \tag{11}$$

where a zero value indicates a perfect symmetry with respect to  $t = 2100$  as for the external forcing. Since, in general, for all models  $A_t(EPRI^2) < A_t(\Delta M_{\delta\Omega})$  with  $A_t(EPRI^2) \approx 0$  (Fig. 9), we can assess that atmospheric changes occur roughly at the same time scale as the external forcing, while the ocean adjustments through freshwater advection are time lagged. This out-of-phase response between EPRI and advective terms is what eventually determines a net freshening, i.e.  $M_t > 0$  or salinification, i.e.  $M_t < 0$  in the boxes. More precisely, when the radiative forcing increases, the EPRI immediately grows (diminishes) in the MA and SA (NA), while advective adjustments

are slower. This determines a net salinification (freshening) in the MA and SA (NA) during the ramp-up. The salinity recovery depends on (i) the degree of inertia of advective terms and (ii) the way in which the ocean responds to the salinity anomaly in different regions. Both cases will be analysed hereafter.

#### 4.2 The inertia of the oceanic system

We outline the role of inertia in determining different evolutions of  $S_t^* = - \int_t M_t^{\Omega}(t) dt$  in a generic box  $\Omega$  with the assistance of a simple conceptual model, where the net inflow/outflow of freshwater is determined by a generic component EPRI symmetric to  $t_0$  (which corresponds to 2100 in our experiments) that is compensated by an asymmetric component OCE. The former is representative of the freshwater fluxes at the surface while the latter gathers all the advective and diffusive terms. Figure 10 shows two different idealized responses of OCE (blue lines) under a same response of EPRI (green line) such that, for both cases,  $\int_{t_i}^{t_f} OCE(t) dt = - \int_{t_i}^{t_f} EPRI(t) dt$ , where  $t_i$  and  $t_f$



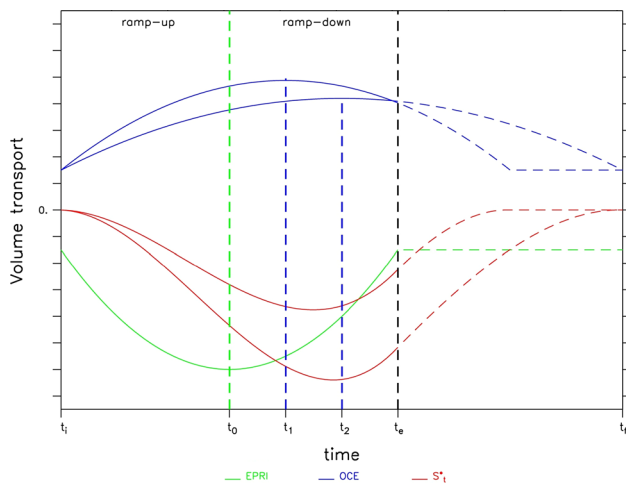


**Fig. 10** Conceptual representation of 2 different time-scale responses of the OCE term (*blue lines*) in conjunction with the same EPRI term (*green line*), and the corresponding  $S_t^*$  evolution (*red lines*, here scaled). The EPRI is assumed to be symmetrical in time to the value  $t_0$  on t-axis which ideally corresponds to year 2100 in our experiments. The values  $t_i$  and  $t_e$  are the equivalents of the beginning of the ramp-up and the end of ramp-down experiments, respectively, while  $t_f$  is the final time of integration after an equilibrium is reached. The values  $t_1$  and  $t_2$  correspond to the axis of symmetry of the two different OCE signals with  $t_1 < t_2$

ideally indicate, respectively, an initial and final time of integration, when an equilibrium is reached. Starting from an equilibrium condition at  $t_i$ , it is clear that the transient response of  $S_t^* = \int_{t_i}^t (EPRI(t) + OCE(t)) dt$  (red lines) is strongly dependent on the degree of asymmetry with respect to  $t_0$  of the term OCE. In particular, a higher inertia of the OCE term can determine a stronger reduction of  $S_t^*$ , associated with lower values at the end of the ramp-down.

As already shown in Fig. 2, the major source of salinity anomaly accomplished by changes in hydrological cycle during the warming scenario is the one in the MA. Hence, an indication of the different degrees of inertia shown by the models can be inspected by evaluating (i) the capacity of each model in opposing changes directly induced by external forcing, and (ii) the rapidity in re-establishing the initial condition in the MA once the radiative forcing is reversed. Figure 11 illustrates the evolution  $M_t^{MA}$  where the negative (positive) filled regions indicate the total amount of freshwater loss (gain) into the MA. For all models, the ramp-up phase is characterized by a salinity rise (negative  $M_t^{MA}$ ) within the MA. This trend continues also for part of the ramp-down phase, notably for HadGEM2-ES and IPSL-CM5A-LR, in which a freshening starts to take place only at the end of the experiment (positive  $M_t^{MA}$ ). The ratio between salinification/freshening, i.e. negative filled portion/positive filled portion in Fig. 11, reported in Table 3 suggests that for HadGEM2-ES and IPSL-CM5A-LR there is more “resistance” compared to EC-EARTH and

MPI-ESM-LR in releasing the amount of salinity anomaly generated in MA during the ramp-up experiment.

This different *inertia* can be inspected in the AMOC index of Fig. 4. By considering  $\Omega$  as NA–SA, it is possible to study the evolution of AMOC through the  $S_t^*$  term. Hence, in this case,  $S_t^*$  is directly related to meridional salinity contrast  $\Delta S_{NA-SA}$  and, in turn, to  $\Delta \rho_{NA-SA}$  and AMOC. Different inertia of the OCE terms determine different behaviours of  $S_t^*$ . More inertial models are indeed those in which the AMOC reduces most during the ramp-up and those with a slower recovery. The evidence that most of the salinity anomaly still remains within the MA for all models suggests that longer simulations with a stabilized radiative forcing can possibly temporarily enhance the AMOC for EC-EARTH and MPI-ESM-LR further and can potentially trigger a (shifted in time) AMOC overshoot even in HadGEM2-ES and IPSL-CM5A-LR.

### 4.3 Different responses of freshwater advection in NA and SA

If applied to the meridional salinity contrast, i.e.  $\Omega = NA - SA$ , the conceptual analysis presented in Fig. 10 can only partially explain the behaviour of the AMOC. Indeed, it assumes that the salinity recovery within NA and SA occurs at the same time, as the OCE term is symmetric to  $t_1$  or  $t_2$  (see Fig. 10). However, the models can adjust in different ways at the boundaries of NA and SA, meaning that an out-of-phase response between NA and SA may arise. In order to account for this, in Fig. 10 the decompositions  $EPRI = EPRI_{NA} - EPRI_{SA}$  and  $OCE = OCE_{NA} - OCE_{SA}$  enables to analyze the response of  $\Delta S_{NA-SA}$ , i.e.  $S_t^*$ , under un-synchronized oceanic components. In this conceptual framework, the delayed response of the SA with respect to NA produces an overshoot of  $\Delta S_{NA-SA}$  that can occur as early as during the ramp-down phase (Fig. 12a), while, in the opposite case, the meridional salinity contrast needs more time to recover (Fig. 12b) without showing any overshooting.

In order to test the conceptual validity of such a simplified model, we have reconstructed the OCE and EPRI terms from the model outputs by using a 2nd degree interpolating polynomial as shown in Fig. 13. Furthermore, for the generic box  $\Omega$ , we have defined the parameter  $T_R^\Omega$  as

$$T_R^\Omega : \int_{t=0}^{T_R} OCE^\Omega dt = \int_{t=0}^{T_R} EPRI^\Omega dt \quad (12)$$

which gives the time needed for the oceanic component to balance the salinity anomaly due to EPRI term. By assuming EPRI changes occurring at the same time as the external forcing, i.e. symmetric to 2100,  $T_R^\Omega$  indicates the different inertia shown by the oceanic components. It is therefore possible to pinpoint its faster response in NA (SA) with

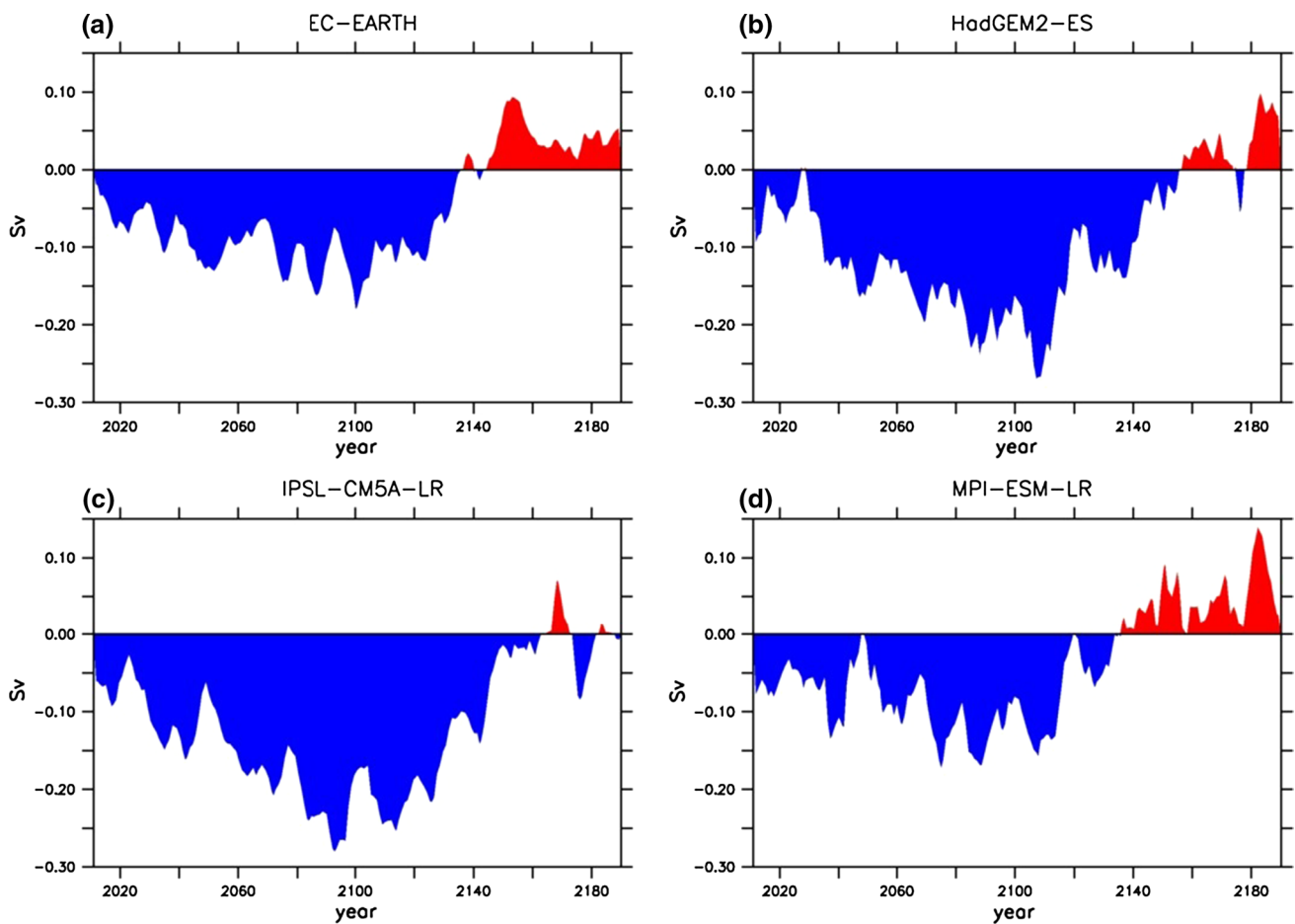


**Fig. 11** Evolution of the term  $M_t^{MA}$  of Eq. 10 for **a** EC-EARTH, **b** HadGEM2-ES, **c** IPSL-CM5A-LR and **d** MPI-ESM-LR. The negative

region (blue) represents the salinity anomaly build-up in MA during the warming scenario, while the positive region (red) indicates the freshening trend after the reversal of the radiative forcing

**Table 3** Quantification of the total volume of equivalent freshwater entering and leaving the MA

Model	Outflow ( $\times 10^{14} \text{m}^3$ )	Inflow ( $\times 10^{14} \text{m}^3$ )	Ratio (inflow/outflow) (%)
EC-EARTH	3.84	0.69	17.9
HadGEM2-ES	6.02	0.41	6.80
IPSL-CM5A-LR	7.10	0.10	1.47
MPI-ESM-LR	3.47	0.88	25.5

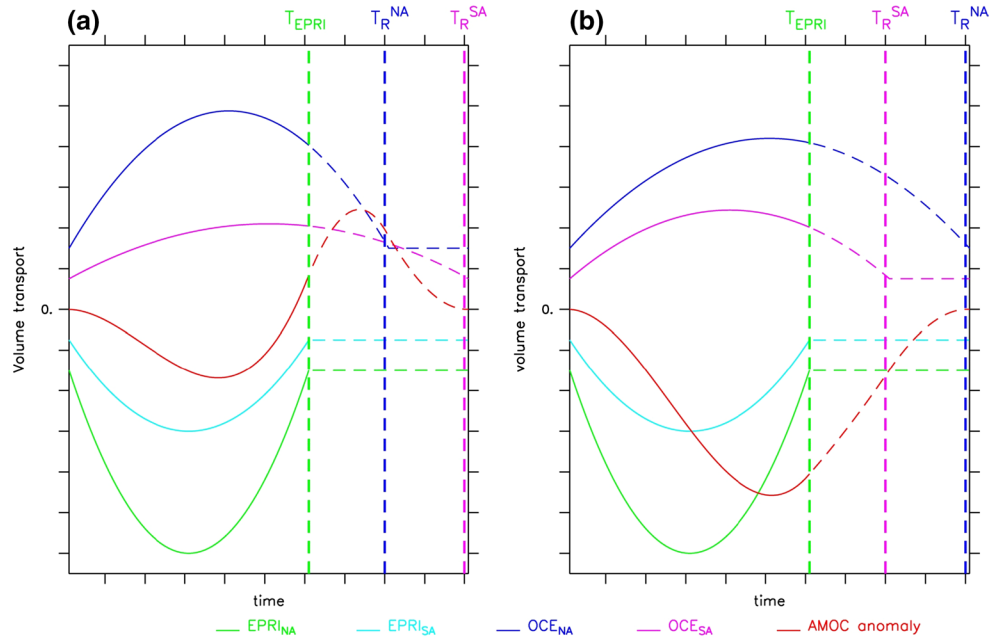
The net inflow (outflow) is calculated as the sum of the positive (negative) imbalances in Eq. 10 during the simulations and corresponds to the integral of the positive (negative) portions in Fig. 11

respect to the one in SA (NA) if  $T_R^{NA} < T_R^{SA}$  ( $T_R^{NA} > T_R^{SA}$ ). As evidenced in Fig. 13, for EC-EARTH and MPI-ESM-LR the response of OCE terms in NA ( $T_R^{NA}|_{EC-EARTH} = 2175$ ,  $T_R^{NA}|_{MPI-ESM-LR} = 2183$ ) is faster than in SA ( $T_R^{SA}|_{EC-EARTH} = 2191$ ,  $T_R^{SA}|_{MPI-ESM-LR} = 2191$ ), while the opposite behaviour can be found for HadGEM2-ES ( $T_R^{NA}|_{HadGEM2-ES} = 2194$ ,  $T_R^{SA}|_{HadGEM2-ES} = 2190$ ) and

IPSL-CM5A-LR ( $T_R^{NA}|_{IPSL-CM5A-LR} = 2193$ ,  $T_R^{SA}|_{IPSL-CM5A-LR} = 2184$ ). Hence, we assert that different behaviours found in the model outputs are the consequence of different inertia of the ocean in the NA and SA. Furthermore, it is worth noting that for EC-EARTH and MPI-ESM-LR the oceanic response in NA is even faster than the atmospheric one being  $T_R < 2190$ . This explains the salinity overshoot in the region shown in Fig. 7a, d. During the ramp-up phase, changes in the hydrological cycle induce a strong salinification in the MA in opposition to a general freshening elsewhere. Hence, beyond what concerns the NA and SA, once the external forcing is reversed, the recovery process must also re-adjust the salinity loss in the Pacific and Indian Ocean. The latter can be achieved through a salinity flux from the MA towards the rest of the ocean, either across the NA or/and SA.

Depending on the “preferential path” established in releasing elsewhere the salinity anomaly previously stocked within the MA, a temporarily anomalous strong salinity could arise within the NA or/and SA during the transient

**Fig. 12** Conceptual evolution of  $\Delta AMOC = kS_t^* = k \int_{t_{im}}^t (OCE_{NA} + EPRI_{NA} - OCE_{SA} - EPRI_{SA}) dt$  (red line), where  $k$  is an empirical scaling constant, under different out of phase responses of the EPRI terms (green and cyan lines) and OCE terms (blue and violet lines). **a** faster response in the NA; **b** faster response in the SA.  $T_{EPRI}$  corresponds to the end of ramp-down, i.e. when the EPRI terms become constant, while  $T_R^\Omega$  refers to Eq. 12, with  $\Omega = NA$  or SA



phase. This supplementary factor affects the NA–SA salinity contrast during the ramp-down if the oceanic adjustments mainly support an additional salinity transport in the NA (SA). To indicate the prevailing trend in releasing the salinity anomaly in the MA, we applied the asymmetrical linear operator defined in Eq. 11 to the divergence of the inflowing freshwater advection in MA

$$A_t(-\text{div} \Delta M_{MA}) = A_t(\Delta M_{48} - \Delta M_{34}) = \Delta M_{48}^{DW} - \Delta M_{34}^{DW} - \Delta M_{48}^{UP} + \Delta M_{34}^{UP} \quad (13)$$

A positive value of  $A_t(-\text{div} \Delta M_{MA})$  suggests the prevalence of a northward salinity anomaly transport after the external forcing is reversed, while a negative sign indicates the opposite trend. Figure 14 shows the single contribution of each term in Eq. 13. For EC-EARTH and MPI-ESM-LR the asymmetry measure indicates a main predisposition in advecting the salinity anomaly formed in the MA northward. This is responsible for the salinity overshooting within the NA for EC-EARTH and MPI-ESM-LR (Fig. 7). On the other hand, the negative values found for  $A_t$  in HadGEM2-ES and IPSL-CM5-LR suggest a prevailing southward path in releasing the salinity anomaly in MA.

By following the same approach used in Eq. 5, the decomposition of the advective term  $\Delta M_{\delta\Omega}$  into

$$\Delta M_{\delta\Omega} = M_{\delta\Omega} + T_{\delta\Omega} = M_{OV}^{\delta\Omega} + M_{AZ}^{\delta\Omega} \quad (14)$$

where the  $\delta\Omega = 48^\circ\text{N}$  or  $34^\circ\text{S}$ , enables to recognize the importance of the overturning and the azonal term in determining the sign of  $A_t(-\text{div} \Delta M_{MA})$ . In Fig. 14, the contribution of these components are detailed. For EC-EARTH, an increase of both  $M_{OV}$  and  $M_{AZ}$  at  $48^\circ\text{N}$  contributes in

determining a positive  $A_t(-\text{div} \Delta M_{MA})$ , with the azonal component playing a major role. For HadGEM2-ES, the resulting southward preferential path for the advection of the salinity anomaly in the MA is essentially driven by a strong increase of  $M_{AZ}$  at  $34^\circ\text{S}$ . In a similar way, for IPSL-CM5A-LR the azonal freshwater transport evolution at the southern boundary of MA is decisive for a negative  $A_t(-\text{div} \Delta M_{MA})$ . Moreover, for this model, a decrease of  $M_{AZ}$  at  $48^\circ\text{N}$  also plays an important role in favouring a negative  $A_t(-\text{div} \Delta M_{MA})$ . The overturning transport of freshwater at  $48^\circ\text{N}$ , on the contrary, is the crucial component in determining a massive northward salinity transport for MPI-ESM-LR during the ramp-down phase, while the  $M_{AZ}$  at  $48^\circ\text{N}$  also contributes to such a behaviour but to a lesser extent.

There is no a leading common factor in determining the different responses at MA boundaries. The  $M_{OV}$  changes affect only those models for which  $A_t(-\text{div} \Delta M_{MA})$  is positive. Nevertheless, changes in the azonal circulation are shown to play a role in all cases. Furthermore, the latter component is decisive in determining the final behaviour in releasing the MA salinity anomaly for three models. Hence, in our 190-year transient experiment, the AMOC restoring processes are generally not dominated by overturning circulation feedbacks, but rather by changes in freshwater transport from the gyres.

### 5 Conclusions and discussion

In this paper, a comparison between 4 different global climate models (EC-EARTH, HadGEM2-ES, IPSL-CM5A-LR

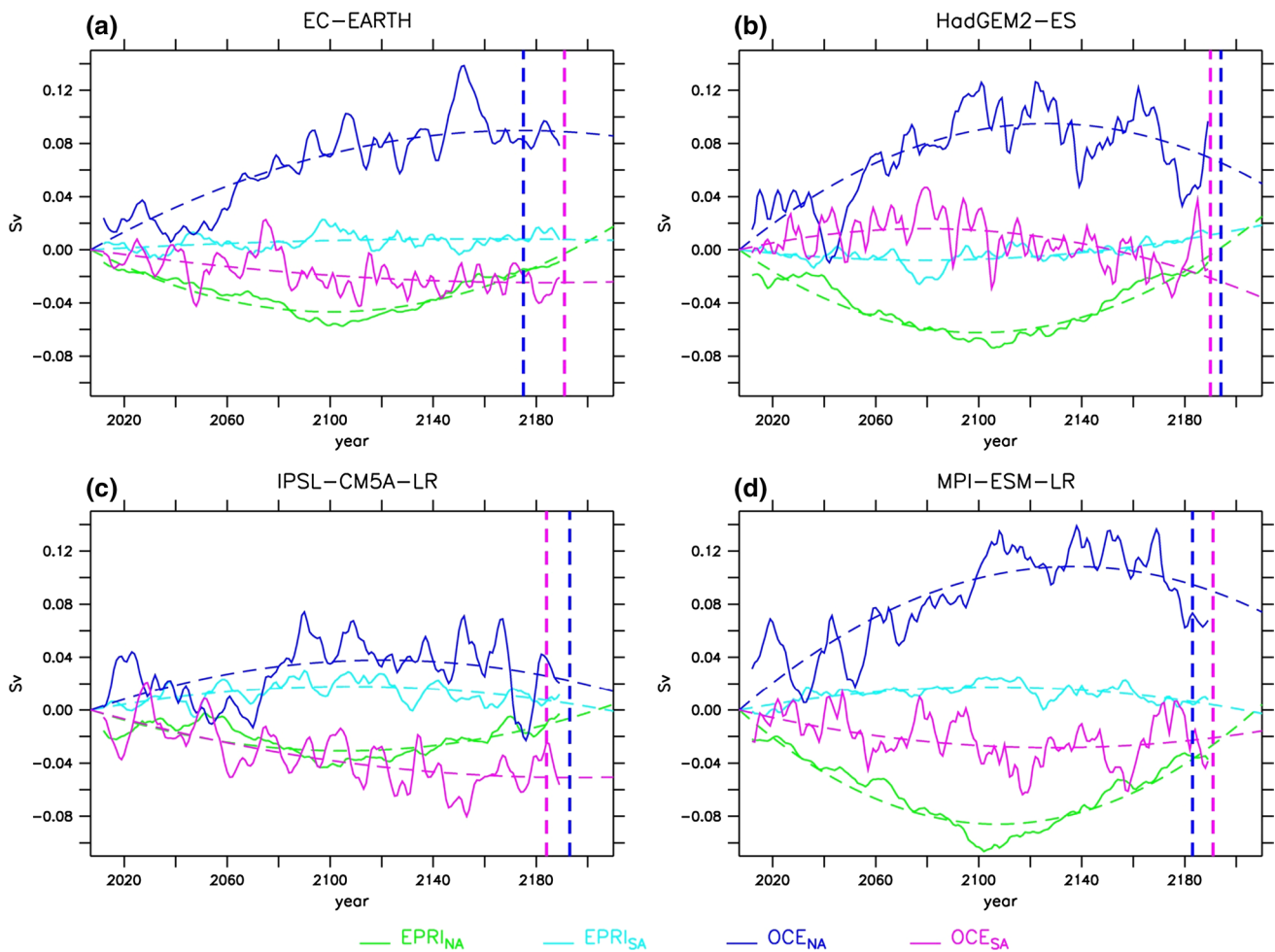


**Fig. 13** Reconstruction of the EPRI anomaly (green for the NA and cyan for the SA) and OCE anomaly (blue for the NA and violet for the SA) terms and respective  $T_R^Q$  (dashed vertical blue and violet lines). It must be noted that the initial values of EPRI terms do not match the corresponding initial value of OCE terms, with in general

$EPRI_{t=2006} > -OCE_{t=2006}$  (not visible here). It means that advective and atmospheric terms are not in equilibrium at the beginning of our experiments. This is because the externally forced warming trend already started during the historical simulation

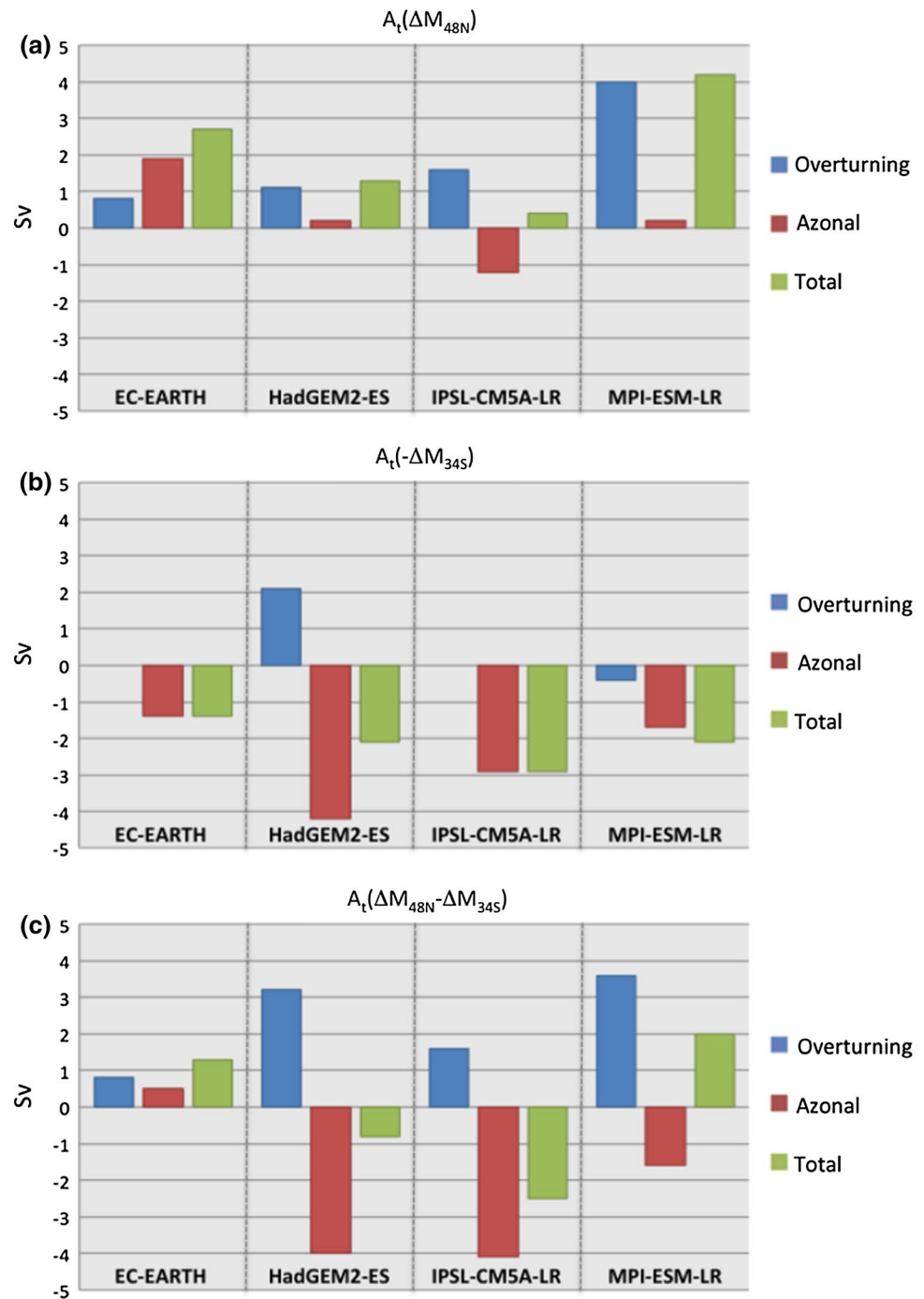
and MPI-ESM-LR) was performed for a future climate projection, in which a RCP8.5 scenario until 2100 was followed by a symmetrical reversal of the external forcing up to 2195.

For all models, a reduction of the AMOC strength occurred during the RCP8.5 warming scenario, but no abrupt collapse has been reported. The amount of AMOC reduction ranged from 25 to 35 % in accordance with other model intercomparisons (Weaver et al. 2012). The reversal of the radiative forcing generally strenghtens the AMOC. Two models, i.e. EC-EARTH and MPI-ESM-LR, experience an overshoot within 2195. For the IPSL-CM5A-LR, the AMOC recovery does not occur clearly and its decreasing trend lasts throughout roughly half of the ramp-down experiment. It must be stressed that the initial value of the AMOC for IPSL-CM5A-LR is too weak if compared to observations and other model outputs. There is a potential analogy with the multimodel analysis carried out by

Weaver et al. (2012), in which the two models with the weakest initial AMOC were characterised by a complete extinction of the AMOC after more than 200 years of stabilization of the RCP8.5 radiative forcing scenario.

Different responses of the AMOC are associated to different evolutions of the density within the NA, the MA and the SA. In our investigation we considered the full-depth density change in each box. Hence, we did not account for vertical adjustments, which can effectively determine different responses among the models. However, this issue would deserve a detailed analysis in future studies. Changes in hydrological cycle, i.e. more precipitation in the North Atlantic, and in temperature field, i.e. a warmer North Atlantic, are both important in reducing the density in the deep water formation region and the production of NADW under a global warming scenario. During the ramp-up phase, a higher temperature in the NA is generally the

**Fig. 14** Contribution of the overturning and azonal components in determining the sign of  $A_t(-\text{div}\Delta M_{MA})$  as detailed in Eq. 13: **a** asymmetry of  $M_{48N}$ , **b** asymmetry of  $M_{34S}$  and **c** asymmetry of the divergence, i.e.  $A_t(-\text{div}\Delta M_{MA})$



primary cause of a decline of density in this region. This is in agreement with the analysis of Gregory et al. (2005) in which they reported an AMOC decrease under global warming experiments mainly driven by changes in surface thermal fluxes rather than by surface freshwater fluxes. However, by considering the AMOC as controlled by a meridional density contrast, the freshwater fluxes become of primary importance both for the ramp-up (in agreement with Dixon et al. 1999) and for the ramp-down phase. In our density budgeted it was pointed out that  $\Delta\rho_{NA-SA}$  is

mainly controlled by the haline components. Indeed, the recovery process of the overturning circulation strength is supported by an increase in the salinity differences between NA and SA during the ramp-down. In particular, the causes of the AMOC overshoot in EC-EARTH and MPI-ESM-LR are related to an exceeding increase of  $\Delta S_{NA-SA}$ .

We proposed a simple conceptual box model which geometrically corresponds to the interhemispheric Stommel box model. Considering the salinity budget within each box regulated by EPRI (which takes into account changes in



hydrological cycle) and OCE (which includes adjustments *via* ocean advection and diffusion), we showed that their out-of-phase response to an external ramp-up/ramp-down forcing theoretically explains the main model differences. We found that the OCE response in HadGEM2-ES and IPSL-CM5A-LR in releasing salinity from the MA to the NA was slower than the one in EC-EARTH and MPI-ESM-LR. These different inertia explain the different reductions in AMOC strength at the end of the ramp-up experiment. Moreover, a faster response of the OCE terms in the NA than in the SA can possibly support an exceeding meridional salinity gradient favouring an AMOC overshoot as shown in EC-EARTH and MPI-ESM-LR. In those models, additional salinity advection to the NA further accelerates its recovery process leading to an anomalously high salt content.

Oceanic adjustments play an important role in determining the response of AMOC in ramp-up/ramp-down experiments. Different behaviours shown by the models are the consequence of different inertia in restoring initial conditions once the radiative forcing is reversed. These model differences may have different reasons. We exclude that the main cause is related to biases of the wind stress. Indeed, no strong difference has been evidenced in comparing wind stress of the different models (not shown). As detailed in Swingedouw et al. (2013), the asymmetry between subpolar and subtropical gyre may determine the amount of freshwater leakage from the North Atlantic while it is perturbed by a negative salinity anomaly. Although their findings regard hosing experiments around Greenland, we can infer that the same underlying processes are qualitatively valid for the experiments here presented. Moreover, freshwater exchanges at the Equator can also play a role in determining different inertia. By dividing the MA box into a northern part (MAN), i.e. the part in the North Hemisphere, and a southern part (MAS), i.e. the one in the South Hemisphere, we noticed that a similar amount of evaporation anomaly in the MAS among the models did not correspond to a same salinity anomaly in the region. For HadGEM2-ES and IPSL-CM5A-LR, the salinity increased during the ramp-up while for EC-EARTH and MPI-ESM-LR the salinity remained nearly constant during the entire experiment. This indicates that for the latter two models, water exchanges yield a northward salinity flux in the MAN, where interactions with North Atlantic subtropical gyre eventually favour a faster NA salinity recovery.

The way in which the AMOC recovers is related to the salinification of the MA during the ramp-up as already shown in Wu et al. (2011) and Jackson et al. (2014). In particular, by comparing the results of 11 different experiments, Jackson et al. (2014) proposed the amount of salinity anomaly overstocked in the upper layer of the subtropical North Atlantic during the warming scenario as an indicator

of the amount of AMOC overshoot to follow later. They indeed found a significant correlation, i.e. 0.71, between the amount of AMOC overshoot among the models and their corresponding subtropical North Atlantic salinity accumulation during the ramp-up. The physical reason behind this is that most of the salinity anomaly formed in the subtropical North Atlantic, is more likely released in the deep water formation region once the external forcing is reversed. However, here we did not find the same significant correspondence between AMOC anomaly at the end of the experiments and the ramp-up salinity accumulation in the upper subtropical North Atlantic. We infer that such a lack of correspondence is due to a different salinity accumulation in the tropical South Atlantic. The latter represents a potential salinity source that can be directly advected in the SA during the ramp-down phase. Given the linear dependence of the AMOC on the NA–SA density contrast, a salinity anomaly advected southward of 34°S can eventually have a non-negligible effect on the recovery process. If the indicator proposed by Jackson et al. (2014) is adjusted for the potentially available salinity in the tropical South Atlantic, i.e. by subtracting from the former indicator the salinity anomaly formed during the ramp-up in the Atlantic region between 0° and 34°S, i.e. in the MAS, the correlation between AMOC anomaly and indicator increases from 0.09 to 0.72 in our experiments. Due to the limited numbers of models analysed here, a larger multimodel analysis is needed to test the validity of this indicator.

We find that the salt advection feedback, i.e.  $M_{OV}$ , is of limited importance in determining the AMOC evolution in transient simulations. The negative value of  $M_{OV}$  in IPSL-CM5A-LR seems in agreement with the higher resistance exhibited in the recovery process. Indeed, a positive salt advection feedback may inhibit the restoration of the initial density in the NA. However, for being a robust indicator for this transient behaviour,  $M_{OV}$  should weaken in response to a slowing AMOC. In IPSL-CM5A-LR this does not occur, as the overturning circulation increasingly imports saltier water in the Atlantic despite its reduction in strength. This is likely to be due to changes in the background salinity field as a consequence of a general salinification of the Atlantic (Swingedouw et al. 2007), thus evidencing that other factors (as atmospheric feedbacks or gyre circulation changes) may overwhelm the salt advection feedback to an AMOC slowing. Due to the multiplicity of the processes involved, we infer that  $M_{OV}$  cannot effectively predict the AMOC evolution in response to large changes in radiative forcing. Indeed, as shown here, the  $M_{OV}$  generally plays only a minor role in determining the  $\Delta S_{NA-SA}$  evolution, i.e. the transient AMOC behaviour. Rather, salinity redistribution within the Atlantic is mainly controlled by gyre circulation adjustments, i.e.  $M_{AZ}$  changes. The only exception concerns MPI-ESM-LR, for which  $M_{OV}$  is the leading

oceanic component in determining the  $\Delta S_{NA-SA}$  evolution. Since the modelled AMOC seems to be weaker than observational estimates in all models but MPI-ESM-LR, there is a possibility that the limited importance of the salt advection feedback we found in EC-EARTH, HadGEM2-ES and IPSL-CM5A-LR is, at least partially, due to an underestimation of the AMOC. Hence, one may speculate that the stronger the overturning circulation, the more important the salt advection feedback. This conjecture may promote wider multi-model analyses.

**Acknowledgments** This research was supported by the Embrace Project, European Union's Seventh Framework Programme for Research Number 282672. For helping to conduct the MPI-ESM ramp-down simulation, we thank Johann Jungclauss and Nils Fischer from MPI-M as well as Joerg Wegner from the German Climate Computing Centre. The authors wish also to acknowledge Jelle van den Berk from KNMI for his support in sorting and archiving EC-EARTH data. We are grateful to two anonymous reviewers for their precious comments.

## References

- Alley RB et al (2003) Abrupt climate change. *Science* 299:2005–2010
- Armour KC, Eisenman I, Blanchard-Wrigglesworth E, McCusker KE (2011) The reversibility of sea ice loss in a state-of-the-art climate model. *Geophys Res Lett* 38(L16):705
- Boucher O et al (2012) Reversibility in an Earth System model in response to CO<sub>2</sub> concentration changes. *Environ Res Lett* 7:024013. doi:10.1088/1748-9326/7/2/024013
- Bouttes N, Gregory JM, Lowe JA (2013) The reversibility of sea level rise. *J Clim* 26:2502–2513
- Broecker WS (1997) Thermohaline circulation, the Achilles heel of our climate system: will man-made CO<sub>2</sub> upset the current balance? *Science* 278:1582–1588
- Bryan F (1986) High-latitude salinity effects and interhemispheric thermohaline circulation. *Nature* 323:301–304. doi:10.1038/323301a0
- Bryden HL, King BA, McCarthy GD, McDonagh EL (2014) Impact of a 30 % reduction in Atlantic meridional overturning during 2009–2010. *Ocean Sci Discuss* 11:789–810
- Bryden HL, Longworth HR, Cunningham SA (2005) Slowing of the Atlantic meridional overturning circulation at 25°N. *Nature* 438:655–657
- Clark PU, Pisias NG, Stocker TF, Weaver AJ (2002) The role of thermohaline circulation in abrupt climate change. *Nature* 415:863–869
- Collins WJ et al (2011) Development and evaluation of an Earth-system model—HadGEM2. *Geosci Model Dev Discuss* 4:997–1062. doi:10.5194/gmdd-4-997-2011
- de Vries P, Weber SL (2005) The Atlantic freshwater budget as a diagnostic for the existence of a stable shut-down of the meridional overturning circulation. *Geophys Res Lett* 32(L09):606. doi:10.1029/2004GL021450
- Dijkstra HA (2007) Characterization of the multiple equilibria regime in a global ocean model. *Tellus A* 59:695–705. doi:10.1111/j.1600-0870.2007.00267.x
- Dixon KW, Delworth TL, Spelman MJ, Stouffer RJ (1999) The influence of transient surface fluxes on the North Atlantic overturning in a coupled GCM climate change experiment. *Geophys Res Lett* 26:2749–2752
- Drijfhout S, van Oldenborgh GJ, Cimadoribus A (2012) Is a Decline of AMOC causing the warming hole above the North Atlantic in observed and modeled warming patterns? *J Clim* 25:8373–8379. doi:10.1175/JCLI-D-12-00490.1
- Drijfhout SS, Weber SL, Swaluw E (2010) The stability of the MOC as diagnosed from model projections for pre-industrial, present and future climates. *Clim Dyn* 37:1575–1586. doi:10.1007/s00382-010-0930-z
- Dufresne J-L et al (2013) Climate change projections using the IPSL-CM5 Earth System model: from CMIP3 to CMIP5. *Clim Dyn* 40:2123–2165. doi:10.1007/s00382-012-1636-1
- Ganachaud A, Wunsch (2003) Large-scale ocean heat and freshwater transports during the World Ocean Circulation Experiment. *J Clim* 16:696–705
- Garzoli SL, Baringer MO, Dong S, Perez RC, Yao Q (2013) South Atlantic meridional fluxes. *Deep-Sea Res* 171:21–32
- Giorgetta MA et al (2013) Climate and carbon cycle changes from 1850 to 2100 in MPI-ESM simulations for the coupled model intercomparison project phase 5. *J Adv Model Earth Syst* 5:572–597. doi:10.1002/jame.20038
- Gregory JM et al (2005) A model intercomparison of changes in the Atlantic thermohaline circulation in response to increasing atmospheric CO<sub>2</sub> concentration. *Geophys Res Lett* 32:L12 703–L12 707
- Hawkins E, Smith RS, Allison LC, Gregory JM, Woollings TJ, Pohlmann H, de Cuevas B (2011) Bistability of the Atlantic overturning circulation in a global climate model and links to ocean freshwater transport. *Geophys Res Lett* 38(L10):605. doi:10.1029/2011GL047208
- Hofmann M, Rahmstorf S (2009) On the stability of the Atlantic meridional overturning circulation. *Proc Natl Acad Sci USA* 106(20):584–589. doi:10.1073/pnas.0909146106
- Hu A, Meehl GA, Han W, Yin J (2011) Effect of the potential melting of the Greenland Ice sheet on the meridional overturning circulation and global climate in the future. *Deep Sea Res* 58:1914–1926. doi:10.1016/j.dsr2.2010.10.069
- Huisman SE, den Toom M, Dijkstra H a, Drijfhout S (2010) An indicator of the multiple equilibria regime of the Atlantic meridional overturning circulation. *J Phys Oceanogr* 40:551–567. doi:10.1175/2009JPO4215.1
- IPCC (2013) Summary for policymakers. In: *Climate change 2013: the physical science basis. Contribution of working group I to the Fifth assessment report on the intergovernmental panel on climate change*, Cambridge University Press, Cambridge, New York
- Jackson LC, Schaller N, Smith RS, Palmer MD, Vellinga M (2014) Response of the Atlantic meridional overturning circulation to a reversal of greenhouse gas increases. *Clim Dyn* 42:3323–3336. doi:10.1007/s00382-013-1842-5
- Johns WE et al (2011) Continuous, array-based estimates of Atlantic Ocean heat transport at 26.5°N. *J Clim* 24:2429–2449
- Kanzow T et al (2010) Seasonal variability of the Atlantic meridional overturning circulation at 26.5°N. *J Clim* 23:5678–5698. doi:10.1175/2010JCLI3389.1
- Lenton TM (2011) Early warning of climate tipping points. *Nat Clim Change* 1:201–209. doi:10.1038/nclimate1143
- Liu W, Liu Z (2013) A diagnostic indicator of the stability of the Atlantic meridional overturning circulation in CCSM3. *J Clim* 26:1926–1938. doi:10.1175/JCLI-D-11-00681.1
- Manabe S, Stouffer RJ (1988) Two stable equilibria of a coupled ocean-atmosphere model. *J Clim* 1:841–866. doi:10.1175/1520-0442(1988)001<0841:TSEOAC>2.0.CO;2
- Manabe S, Stouffer RJ (1993) Century-scale effects of increased atmospheric CO<sub>2</sub> on the ocean-atmosphere system. *Nature* 364:215–218
- Manabe S, Stouffer RJ (1995) Simulation of abrupt changes induced by freshwater input to the North Atlantic. *Nature* 378:165–167

- Meinshausen M et al (2011) The RCP greenhouse gas concentrations and their extensions from 1765 to 2300. *Clim Change* 109:213–241. doi:[10.1007/s10584-011-0156-z](https://doi.org/10.1007/s10584-011-0156-z)
- Nakashiki N, Kim D-H, Bryan FO, Yoshida Y, Tsumune D, Maruyama K, Kitabata H (2006) Recovery of thermohaline circulation under CO<sub>2</sub> stabilization and overshoot scenarios. *Ocean Model* 15:200–217. doi:[10.1016/j.ocemod.2006.08.007](https://doi.org/10.1016/j.ocemod.2006.08.007)
- Rahmstorf S (1996) On the freshwater forcing and transport of the Atlantic thermohaline circulation. *Clim Dyn* 12:799–811. doi:[10.1007/s003820050144](https://doi.org/10.1007/s003820050144)
- Rahmstorf S et al (2005) Thermohaline circulation hysteresis: a model intercomparison. *Geophys Res Lett* 32(L23):605. doi:[10.1029/2005GL023655](https://doi.org/10.1029/2005GL023655)
- Rooth C (1982) Hydrology and ocean circulation. *Prog Oceanogr* 11:131–149. doi:[10.1016/0079-6611\(82\)90006-4](https://doi.org/10.1016/0079-6611(82)90006-4)
- Schmittner A, Latif M, Schneider (2005) Model projections of the North Atlantic thermohaline circulation for the 21st century assessed by observations. *Geophys Res Lett* 32:L23 710. doi:[10.1029/2005GL024368](https://doi.org/10.1029/2005GL024368)
- Sijp WP, England MH, Gregory JM (2012) Precise calculations of the existence of multiple AMOC equilibria in coupled climate models. Part I: equilibrium states. *J Clim* 25:282–298. doi:[10.1175/2011JCLI4245.1](https://doi.org/10.1175/2011JCLI4245.1)
- Sterl A et al (2011) A look at the ocean in the EC-Earth climate model. *Clim Dyn* 39:2631–2657. doi:[10.1007/s00382-011-1239-2](https://doi.org/10.1007/s00382-011-1239-2)
- Stocker TF, Schmittner A (1997) Influence of CO<sub>2</sub> emission rates on the stability of the thermohaline circulation. *Nature* 388:862–865
- Stommel H (1961) Thermohaline convection with two stable regimes of flow. *Tellus* 13:224–230. doi:[10.1111/j.2153-3490.1961.tb00079.x](https://doi.org/10.1111/j.2153-3490.1961.tb00079.x)
- Swingedouw D, Braconnot P, Delecluse P, Guilyardi E, Marti O (2007) Quantifying the AMOC feedbacks during a 2xCO<sub>2</sub> stabilization experiment with land-ice melting. *Clim Dyn* 29:521–534. doi:[10.1007/s00382-007-0250-0](https://doi.org/10.1007/s00382-007-0250-0)
- Swingedouw D, Braconnot P, Marti O (2006) Sensitivity of the Atlantic meridional overturning circulation to the melting from northern glaciers in climate change experiments. *Geophys Res Lett* 33(L07):711. doi:[10.1029/2006GL025765](https://doi.org/10.1029/2006GL025765)
- Swingedouw D, Mignot J, Braconnot P, Mosquet E, Kageyama M, Alkama R (2009) Impact of freshwater release in the North Atlantic under different climate conditions in an OAGCM. *J Clim* 22:6377–6403. doi:[10.1175/2009JCLI3028.1](https://doi.org/10.1175/2009JCLI3028.1)
- Swingedouw D et al (2013) Decadal fingerprints of freshwater discharge around Greenland in a multi-model ensemble. *Clim Dyn* 41:695–720. doi:[10.1007/s00382-012-1479-9](https://doi.org/10.1007/s00382-012-1479-9)
- Taylor KE, Stouffer RJ, Meehl GA (2012) A summary of the CMIP5 experiment design. *Bull Am Meteorol Soc* 93:485–498
- Trenberth KE, Caron JM (2001) Estimates of meridional atmosphere and ocean heat transport. *J Clim* 14:3433–3443
- Tsutsui J, Yoshida Y, Kim D-H, Kitabata H, Nishizawa K, Nakashiki N, Maruyama K (2007) Long-term climate response to stabilized and overshoot anthropogenic forcings beyond the twenty-first century. *Clim Dyn* 28:199–214. doi:[10.1007/s00382-006-0176-y](https://doi.org/10.1007/s00382-006-0176-y)
- Vellinga M, Wood RA (2002) Global climatic impacts of a collapse of the Atlantic thermohaline circulation. *Clim Changes* 54:251–267
- Weaver AJ et al (2012) Stability of the Atlantic meridional overturning circulation: a model intercomparison. *Geophys Res Lett* 39:1–7. doi:[10.1029/2012GL053763](https://doi.org/10.1029/2012GL053763)
- Weijer W, de Ruijter WPM, Dijkstra HA, van Leeuwen P (1999) Impact of interbasin exchange on the Atlantic overturning circulation. *J Phys Oceanogr* 29:2266–2284
- Wu P, Jackson L, Pardaens A, Schaller N (2011) Extended warming of the northern high latitudes due to an overshoot of the Atlantic meridional overturning circulation. *Geophys Res Lett* 38(24):L24 704. doi:[10.1029/2011GL049998](https://doi.org/10.1029/2011GL049998)
- Wu P, Wood R, Ridley J, Lowe J (2010) Temporary acceleration of the hydrological cycle in response to a CO<sub>2</sub> rampdown. *Geophys Res Lett* 37(12):L12 705. doi:[10.1029/2010GL043730](https://doi.org/10.1029/2010GL043730)
- Zhang R, Delworth TL (2005) Simulated tropical response to a substantial weakening of the Atlantic thermohaline circulation. *J Clim* 18:1853–1860